1

2

3

4

Direct and Indirect Evidence for Free Oxygen (O^{2-}) in MO-Silicate Glasses and Melts (M = Mg, Ca, Pb)

7

8

H.Wayne Nesbitt[1], G.Michael Bancroft[2], Grant S. Henderson[3], Ryan Sawyer[1], Richard A. Secco[1]

[1]Dept. of Earth Sciences, Univ. of Western Ontario, London, Ont., Canada N6A 5B7

[2]Dept. of Chemistry, Univ. of Western Ontario, London, Ont. Canada N6A 5B7

[3] Dept. of Earth Sciences, Univ. of Toronto, Toronto, Ontario Canada M5S 3B1

13

14

15

16

17

18

19

20

21

22

23

24

25

Corresponding author: hwn@uwo.ca

27

28   **ABSTRACT**

29   O 1s XPS spectra of a Pb-silicate glass containing 76.6 mol% PbO provide the first

30   accurate, direct measurement of free oxide ion (O^{2-}) in these glasses. O^{2-} constitutes 35($\pm$3)

31   mol% of total oxygen, with NBO and BO constituting respectively, 52 ($\pm$3) and 13($\pm$3) mol%.

32   All ^{29}Si NMR and O 1s XPS results for Pb silicate glasses indicate mol% levels of O^{2-} containing

33   more than ~30 mol% PbO. The O^{2-} abundances are consistent with equilibrium thermodynamic

34   considerations where K ~ 12 for the mass action equation involving NBO, BO and O^{2-}.

35   Raman and ^{17}O NMR spectra of two CaMg-silicate glasses indicate ~ 10 ($\pm$4) mol% O^{2-}

36   in $CaMgSiO_4$ glass and ~ 18 ($\pm$4) mol% O^{2-} in a $Ca_{0.36}Mg_{0.36}Si_{0.28}O_{1.28}$ glass. Oxygen species

37   abundances are calculated using experimental results from 13 separate ^{29}Si NMR, ^{17}O NMR and

38   Raman measurements of Mg-, Ca- and CaMg-silicate glasses. All reveal mol% levels of O^{2-} with

39   ~ 1 to 2.6 mol% in metasilicate glass and ~ 5 to 10 mol% in orthosilicate glass. Recent Raman

40   experimental results also indicate O^{2-} in CaMg-silicate glasses at levels ranging from about 1 to

41   10 mol%. In all there are 23 separate ^{29}Si NMR, ^{17}O NMR and Raman measurements indicating

42   mol% levels of O^{2-} in alkaline earth silicate glasses. Eight recent MD simulations of Mg, Ca and

43   CaMg-silicate glasses include 21 separate simulations over a wide compositional range. All

44   indicate mol% levels of O^{2-} in the glasses demonstrating that the MD simulations and

45   experimental results on these systems are in accord.

46   There are two fundamentally important implications of these studies. First, free oxygen

47   (O^{2-}) is an *essential constituent* of Pb, Mg, Ca and CaMg binary silicate melts and glasses. It is

48   *not* an 'accidental' product associated with glass or melt defects. It is instead, a

49   thermodynamically important constituent of these binary melts (and glasses). Second, where

50   melts are equilibrated, the mass action equation relating BO, NBO and O^{2-} must hold across the

51   *entire* Ca, Mg, CaMg and Pb binary systems, thereby requiring the activities and mole fractions

52   of all three species to be defined and finite in the melts. Free oxygen, however, may be too low

53   to be detected in highly siliceous glasses using conventional spectroscopic techniques.

54   **Keywords:** XPS of glasses, free oxygen in glasses, silicate glasses, Pb-silicate glass, Ca silicate

55   glass, Mg silicate glass, CaMg silicate glass

INTRODUCTION

57   Over the last two decades dramatic developments have occurred in three techniques

58   relevant to the understanding of distribution of species in silicate glasses and melts. Molecular

59   Dynamics (MD) simulations have improved sufficiently that several hundreds to thousands of

60   atoms may be accommodated using various core-shell interatomic potentials, due primarily to

61   greatly improved computational facilities. From these calculations distributions of Q species,

62   oxygen species, and modifier cation speciation have been evaluated, as have structural properties

63   such as bond angles and lengths (e.g., Mountjoy et al. 2011; Pedone et al. 2010; Mountjoy, 2007;

64   Mead and Mountjoy, 2006; Du and Cormack, 2004). There have been similarly dramatic

65   developments in ^{29}Si NMR spectroscopy. The 2D ^{29}Si MAF NMR and allied 2D spectroscopies

66   generally provide better resolution and clearer demarcation of spectral contributions, than do

67   ^{29}Si MAS NMR spectra. Much greater effort has also been directed toward better quantification

68   of the spectral contributions (Davis et al. 2011; 2010; Zhang et al. 1997;1996; Farnan et al.

69   1992). These advances have revealed spectral contributions in some systems which were

70   impossible to detect by ^{29}Si MAS NMR (e.g., Nesbitt et al. 2015a; Davis et al. 2010). As for the

71   third technique, technical breakthroughs in XPS spectroscopy have made it a useful tool to

72   identify oxygen species in silicate minerals (Zakaznova et al. 2008; 2006; 2005). The most

73   important technical advance was in charge compensation of samples (Nesbitt and Bancroft,

74 2014). With successful charge compensation, linewidths of insulators are commensurate with

75 those of conductors and semi-conductors (Nesbitt et al. 2004). Recent advances in understanding

76 of the contributions to linewidths and lineshapes (Bancroft et al. 2009) also aided greatly in

77 interpretation of Si 2p and O 1s spectra collected from binary silicate glasses (Sawyer et al.

78 2015; 2012; Nesbitt et al. 2015b; 2011; Dalby et al. 2007). Here we assess oxygen speciation in

79 Pb, Mg, Ca and CaMg silicate glasses using information from each of the three techniques. We

80 begin with XPS results followed by contributions from NMR, and finally we address recent MD

81 studies.

82 Determination of the concentration of O^{2-} in silicate glasses is required for

83 thermodynamic modelling of melts and glasses, and to understand the kinetics of reaction of

84 silicate glasses and melts with reagents (e.g., H_2O, CO_2 S-species). Free oxide is highly basic

85 compared with NBO or BO and is likely to be the most reactive oxygen species toward most

86 natural reagents (Sawyer et al., 2015). There is also an exceptionally large reservoir of O^{2-}

87 supplied via the polymerization-depolymerization reaction (Eq. 1). Even at the 0.1% level, its

88 consumption by reaction with reagents will be replaced by conversion of NBO to BO + O^{2-}

89 (Eq.1) to maintain equilibrium among the O species (Eq. 2); the polymerization reaction (Eq, 1)

90 is an O^{2-} buffer. With its high reactivity and buffered nature, O^{2-} may be treated as a master

91 variable in silicate melts, much as H^+ (pH) is in aqueous solutions.

92 The oxygen species are related through the polymerization-depolymerization reaction

93 (Fincham and Richardson, 1954):

94 $$BO + O^{2-} \leftrightarrow 2NBO^- \tag{1}$$
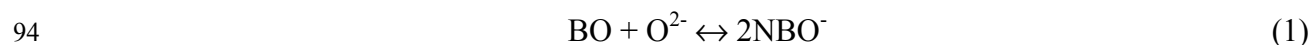
95 where BO represents "bridging" oxygen (Si-**O**-Si; O bonded to two Si atoms), NBO represents

96 "non-bridging" oxygen (Si-**O**-M; O bonded to one Si and a Pb, alkali or alkaline earth atom, M),

4

97   and O^{2-} is free oxygen (M-**O**-M; O *not* bonded to Si but but is also referred to as free oxide, non-

98   network oxygen or non-silica bonded O). The associated mass-action equation is:

99                              $K_1 = (NBO^-)^2/[(BO)(O^{2-})]$ (2)

100   where parentheses indicate activities and K_1 is the equilibrium constant. Early studies

101   demonstrated that K_1 was finite, and that O^{2-} existed in silicate glasses and melts (e.g., Toop and

102   Samis, 1962). Many recent reviews of silicate glasses (e.g., Henderson et al. 2006; Henderson,

103   2005; Mysen, 2003; Stebbins, 1995) do not, however, mention free oxide although many studies

104   published subsequently have reported it in binary silicate glasses (e.g., Al-Hasni and Mountjoy,

105   2014; Sawyer et al. 2015; Nesbitt and Bancroft, 2014; Retsinas et al. 2014; Nasikas et al. 2012;

106   Kohara et al. 2011; 2004; Nesbitt et al. 2011; Davis et al. 2011; Sen et al. 2009; Sen and

107   Tangeman, 2008; Park and Rhee, 2001; Fayon et al. 1998; Zhang et al. 1997). An important

108   objective of this communication is to emphasize the large number of recent studies which

109   indicate O^{2-} in binary silicate glasses.

110   There is good agreement between O 1s XPS and ^{29}Si MAS NMR results, both indicating

111   free oxide (O^{2-}) in Pb silicate glasses (Dalby et al. 2007; Fayon et al. 1998), although it has not

112   been observed directly. We report direct observation of O^{2-} in a glass containing 76.6 mol% PbO.

113   Nasikas et al. (2012) were the first to report direct spectroscopic observation of an O^{2-} signal in

114   binary silicate glasses using ^{17}O NMR spectroscopy. They did not, however, provide fits to these

115   important spectra. The spectra are here deconvoluted using fitting techniques identical to those

116   employed to fit the 76.6 mol% PbO silicate glass, with BO, NBO and O^{2-} abundances evaluated.

117   Zhang et al. (1997) conducted the most exhaustive study of $CaSiO_3$ glass and it remains

118   the benchmark paper for this system. They used a 2D ^{29}Si MAF NMR technique and

119   demonstrated that the glass contained ~ 1 mol% O^{2-}. Thompson et al. (2012) collected ^{17}O NMR

5

120 spectra of a glass containing 56.6 mol% CaO. They concluded that there is "no evidence of free

121 oxide in detectable quantities" and also concluded that free oxide cannot be present at levels

122 greater than 1mol% in glasses containing less than ~ 67 mol% CaO. The issue of O^{2-} abundance

123 in Ca-silicate glasses wants resolution and we address the issue here. Numerous experimental

124 results and MD simulations are reviewed, with O^{2-} contents and uncertainties presented.

EVIDENCE FOR FREE OXIDE FROM EXPERIMENTAL STUDIES

Pb-Silicate Glasses

127 **Experimental Methods and Results:** A glass containing nominally 75 mol% PbO was

128 synthesized according to Dalby et al. (2007). After quenching, minor amounts of small crystals

129 were present at the interface with the sample holder but the interior was glassy. The portion

130 containing the crystals was removed and the interior glass was inspected by SEM (Hitachi

131 SU6600) at magnification of 22,000x. The inspection revealed no inhomogeneities (i.e., no

132 crystals). The sample was analysed by XPS as explained in the next paragraph. After XPS

133 analysis the fragment was coated with carbon and analysed again using an Hitachi SU6600. A

134 synthesized glass containing 67 mol% PbO and a natural olivine crystal (forsterite) were used as

135 standards. Energy dispersive and crystal spectrometer analysis of five spots were averaged

136 yielding 76.6 (±1) mol% PbO. The sample is referred to subsequently as the Pb77 sample.

137 Preparation for XPS analyses consisted of fracturing the glass pellet in the introduction

138 chamber of a Kratos Axis Ultra spectrometer (~10^{-9} Torr) to expose a pristine surface. It was

139 immediately transferred to the analytical chamber (~10^{-10} Torr) and a broadscan was collected.

140 The magnetic confinement charge compensation system was employed as descirbe elsewhere

141 (Dalby et al., 2007; Nesbitt et al., 2011; Sawyer et al., 2012). Details concerning charge

142 compensation are available at 'http://www.kratos.com/products/axis-ultra-dld' and are discussed

6

143   by Nesbitt and Bancroft (2014). High resolution O 1s and Si 2p spectra were collected using 10

144   eV pass energy and conditions described previously (Dalby et al. 2007; Bancroft et al. 2009;

145   Nesbitt et al. 2011, Sawyer et al. 2012). The O 1s spectra shown in Figs. 1a and 1b represent

146   glasses containing 50 mol% PbO (PbSiO$_3$) and 67 mol% PbO (Pb$_2$SiO$_4$), and are from Dalby et

147   al. (2007). The O 1s spectrum of the Pb77 glass (contains 76.6 mol% PbO) is illustrated in Fig.

148   1c. These spectra were fit using a Shirley background (Shirley, 1972) and two peaks (30%

149   Lorentian-70% Gaussian peakshapes) representing BO and NBO+O^{2-} signals. The analytical

150   settings for the Pb77 glass were identical to those used by Dalby et al. (2007) and they should be

151   referred to for details.

152   **Interpretation of O 1s Spectra:**   The fits to the O 1s XPS spectra of Pb-metasilicate (50

153   mol% PbO) and Pb-orthosilicate (67 mol% PbO) glasses (Figs. 1a, 1b) were obtained using the

154   peak fit parameters of Dalby et al. (2007). As for other suites of glasses, all peaks migrate to

155   lower BE with increased metal oxide content as explained by Nesbitt and Bancroft (2014). Two

156   of their findings are very important with respect to this study: (1) the BO linewidths are constant

157   at ~1.22 eV regardless of glass composition; (2) the more intense NBO+O^{2-} peak is composite

158   (Dalby et al. 2007) but its linewidth changes little between 50 and 67 mol% PbO (i.e., 1.17 eV to

159   1.22 eV, Dalby et al. 2007, their Table 2). The effectively constant linewidth of the BO peak

160   (1.22 eV) is expected in that individual peaks contributing to the O 1s spectrum should have a

161   linewidth of ~ 1.25 ±0.1 eV (Bancroft et al. 2009; Nesbitt et al. 2004). It is nevertheless

162   surprising that the composite NBO+O^{2-} peak is just as narrow. As explained by Dalby et al.

163   (2007), the two contributions are effectively superimposed. To summarize, the BO and NBO+O^{2-}

164   peaks are of similar width (~1.22 eV) and are effectively independent of glass composition. This

165   circumstance aids greatly in fitting the O 1s XPS spectrum of the Pb77 glass, as now discussed.

166   **BO% in Pb77 Glass.**   The O 1s XPS spectrum of the Pb77 glass (Fig. 1c) is similar to the

167   orthosilicate glass (Fig. 1b). Both consist of an intense low binding energy (BE) peak with a

168   distinctive shoulder on its high BE side. Using Fig. 1b as guide, the Pb77 glass was fit with a BO

169   and a NBO+O^{2-} peak. As previously discussed the BO linewidth of the Pb77 glass spectrum was

170   constrained to 1.22 eV (Fig. 1c). A second, entirely unconstrained peak was introduced to

171   represent the NBO+O^{2-} contribution and the resulting least squares best fit is shown in Fig. 1c.

172   Fit parameters are listed in Table 1. The fit indicates 10.8 mol% BO with the remainder being

173   NBO+O^{2-}. To evaluate uncertainties, different backgrounds were selected and the BO peakwidth

174   was adjusted by 0.2 eV (i.e., 1.02 and 1.42 eV). No BO value was greater than 2 mol% different

175   from 10.8 mol% and we conclude that BO = 10.8 (±2) mol%. If the polymerization reaction (Eq.

176   1) had gone to completion, all BO would have been consumed. Clearly the reaction did not go to

177   completion leaving some BO and O^{2-} unconsumed. Knowing the glass composition, the BO

178   abundance (10.8%) and the stoichiometry of reaction (1), then following Sawyer et al. (2015, see

179   their section entitled 'Constraints on Oxygen Speciation') the abundances of the three oxygen

180   species can be calculated and these are BO = 10.8 mol%, NBO = 54.2 mol% and O^{2-} = 35.0

181   mol%. A 2 mol% uncertainty is assigned to these values.

182   **Deciphering the NBO+O^{2-} Signal.** The full width at half maximum (FWHM) of the NBO+O^{2-}

183   peak (Fig. 1c) is much broader (1.60 eV) than any other NBO+O^{2-} peak fitted to the Pb-silicate

184   glasses of Dalby et al. (2007). The explanation may relate to the increased intensity of the O^{2-}

185   contribution relative to the NBO contribution and to a shift of the O^{2-} peak to lower BE relative

186   to the NBO peak (with increased PbO content). The hypothesis is now tested. It is evident from

187   Fig. 1c that introduction of separate, unconstrained NBO and O^{2-} peaks will not provide a

188   meaningful fit because there are no features with which to 'fix' the positions, linewidths or

189   intensities of the two peaks. Constraints must be used if the NBO and O^{2-} contributions are to be

190   separated. We have consequently fit the spectrum using three peaks and *two* distinct constraints.

191   By the first method, both BO *and* NBO peaks were constrained at 1.22 eV, as observed in

192   the 67 mol% PbO glass (Fig. 1b). The third (O^{2-}) peak was introduced and was entirely

193   unconstrained. The resulting least squares fit is shown in Fig. 2a with fit parameters listed in

194   Table 1. The fit indicates that the unusual breadth of the NBO+O^{2-} peak is the result of an intense

195   O^{2-} contribution which overlaps the NBO peak. The O-species proportions derived from the fit

196   are BO = 14.7 mol%, NBO = 51.0 mol% and O^{2-} = 34.3 mol%. These compare favourably with

197   the results derived from Fig. 1c where BO = 10.8 mol%, NBO = 54.2 mol% and O^{2-} = 35.0

198   mol%. As evidence for a reasonable fit, an O 1s spectrum of PbO collected by Dr. Mark

199   Biesinger (Surface Science Western, pers. comm.) indicates that its O^{2-} peak is centered at 529.0

200   eV compared with 529.04 eV (for the O^{2-} peak of Fig. 2a (Table 1).

201   For the second deconvolution method, the linewidth of the BO peak is constrained to 1.22

202   eV (as for the first method). The second constraint has the BO, NBO and O^{2-} proportions equal

203   to the values from the two peak fit of Fig. 1c. With BO linewidth constrained to 1.22 eV and

204   with the three peak areas constrained (i.e., BO:NBO:O^{2-} = 10.8%:54.2%:35%), the fit shown in

205   Fig. 2b is obtained. The fit parameters are listed in Table 1. The NBO linewidth is 1.52 which is

206   somewhat greater than 1.25 ±0.1 eV (the value expected from theory, Bancroft et al. 2009;

207   Nesbitt et al. 2004). The O^{2-} peak maximum (529.22 eV) is, however, still close to that expected

208   for O of PbO (529.0 eV, see previous paragraph). Moreover, the fit is similar to the fit of Fig. 2a

209   although different constraints were used, thus providing confidence that deconvolution of the

210   oxygen signals are reasonable.

211   The O^{2-} peak are not evident in Figs. 1a or 1b so that its BE must be < 0.5 eV of the

9

212   respective NBO peak as emphasized by Nesbitt and Bancroft (2014, see their Fig. 13). For the

213   Pb77 glass (Fig. 2), the O^{2-} peak is at 0.5 to 0.7 eV lower BE than the NBO peak in the Pb77

214   glass (Fig. 2). As explanation, all peaks shift to lower BE (and at different rates) with increased

215   counter oxide content (e.g., Nesbitt and Bancroft, 2014, their Fig. 20). The O^{2-} peak of Fig. 2,

216   apparently shifts slightly more than the NBO (Fig. 2), although the energy splitting remains

217   small (0.5 to 0.7 eV). The explanation for this small differential shift is uncertain, but

218   undoubtedly relates to electron density over the NBO and O^{2-} moieties. As PbO increases beyond

219   67 mol%, NBO abundance decreases leaving O^{2-} to take on ever greater electron density and

220   approach the BE of O^{2-} observed in PbO. This aspect, however, needs further study.

221   We conclude that: (1) these types of constraints yield reasonable fits to the Pb77 glass O

222   1s XPS spectrum; (2) the breadth of the NBO+O^{2-} peak of Fig. 1c is indeed the result of an

223   intense O^{2-} peak split from the NBO peak by about 0.5 to 0.7 eV; (3) there is a large amount of

224   O^{2-} in the Pb silicate glasses studied (~35 mol% in Pb77 glass).

225   **Other Experimental Evidence.** Furukawa et al. (1978) and Iwamoto et al. (1979) conducted

226   Raman spectroscopic studies of Pb-silicate glasses and detected BO, NBO and O^{2-} in the high-

227   PbO glasses but amounts are uncertain due to ambiguity in sensitivity factors. Smets and

228   Lommen (1982) conducted an O 1s XPS study of Pb-silicate glasses ranging in composition

229   from 30 to 70 mol% PbO. Their spectra are poorly resolved but their estimates of X_{BO} are similar

230   to those of Dalby et al. (2007), although they display greater variability. The MD and EXAFS

231   study of Rybicki et al. (2001) demonstrated the presence of PbO_4 and possibly PbO_3 groups (i.e.,

232   O^{2-}) in a wide compositional range of Pb-silicate glasses. Takaishi et al. (2005) identified O^{2-} in

233   Pb-silicate glasses using X-ray and neutron diffraction techniques where O is bonded to three Pb

234   atoms. Fayon et al. (1998) observed Q^2 and Q^1 species in invert Pb-silicate glasses (i.e., MO > 50

10

235   mol%). The presence of these Q-species necessitates the presence of O^{2-} in all glasses they

236   reported. Very recently, Lee and Kim (2015) reported O^{2-} in their ^{17}O NMR spectrum of Pb-

237   silicates but they provide neither fits to their spectra nor other support for their quoted O^{2-}

238   abundances. In summary, free oxygen has been detected in Pb-silicate glasses using a wide range

239   of experimental and simulation techniques and there is excellent agreement among the various

240   techniques and laboratories.

241   **Thermodynamic Analysis.** A melt at equilibrium necessarily requires adherence to the mass

242   action equation (Eq. 2) and substitution of mole fractions (X_{NBO}, X_{BO}, X_{O2-}) for activities makes

243   K_1 (Eq. 2) a 'conditional equilibrium constant'. Dalby et al. (2007) report atomic % of oxygen

244   species from which X_{BO}, X_{NBO} and X_{O2-} were calculated. X_{BO} is plotted as a function of glass

245   composition on Fig. 3 (large shaded circles). The large shaded squares (Fig. 3) represent X_{BO}

246   values derived from ^{29}Si NMR Q-species distributions reported by Fayon et al. (1998) and

247   calculated according to Sawyer et al. (2015, see their Appendix A). The large solid circle of Fig.

248   3 represents X_{BO} obtained from the fit to the O 1s XPS spectrum of the Pb77 glass (Fig. 1c). The

249   horizontal error bar represents the uncertainty in the glass composition. The NMR and XPS

250   agreement is reasonable. Both sets of results indicate that the polymerization reaction (Eq. 1)

251   does not go to completion and that $K_1 \sim 12$ (Eq. 2). Values for X_{O2-} of Pb-silicate glasses are, for

252   the first time, presented in Fig. 3 (small symbols). They were calculated from these results for

253   Pb77 glass, the XPS and NMR results of Dalby et al. (2007) and Fayon et al. (1998) using the

254   approach of Sawyer et al. (2015, p. 2). X_{O2-} increases systematically with increasing PbO content

255   and they straddle the X_{O2-} curve calculated for $K_1 = 12.0$. We emphasize that with $K_1 \sim 12.0$,

256   equilibrium (Eq. 2) requires the Pb77 glass to contain about 33 mol% O^{2-} (i.e., $X_{O2-} \sim 0.33$). The

257   two peak fit to the Pb77 glass (Fig. 1c) yields $X_{BO} = 0.108$ and $X_{O2-} = 0.35$. The two fits using

11

258   constraints (Figs. 2a and 2b) also yield oxygen species abundances consistent with $K_1 \sim 12$. The

259   concentration of O^{2-} is reasonably known as a function of composition in the Pb-silicate binary

260   system.

Mg-Ca-Silicate Glasses

262   **Introduction.** Nasikas et al. (2012; 2011) were the first to report direct experimental evidence

263   for O^{2-} in Ca-Mg silicate glasses of composition $Ca_{1.0}Mg_{1.0}Si_{1.0}O_4$ (i.e., CMS33; $SiO_2 = 33$

264   mol%) and $Ca_{1.44}Mg_{1.44}Si_{0.56}O_4$ (CMS28; $SiO_2 = 28$ mol%). The measurement at the orthosilicate

265   composition (CMS33) is particularly instructive because a stoichiometric constraint unique to

266   this composition permits determination of the abundance of all oxygen species provided the

267   concentration of any one species is known. Consider, for example, addition of CaO to SiO_2 melt.

268   Progressive addition of CaO results in BO and O^{2-} being converted to NBO according to Eq. (1)

269   where the BO is derived from SiO_2 and O^{2-} from CaO. If, *at the orthosilicate is composition* the

270   polymerization reaction (Eq. 1) goes to completion, all BO and O^{2-} will be consumed

271   simultaneously and only NBO will be present in the glass. If, however, the reaction does not go

272   to completion, then some BO *and an equal amount of O^{2-}* will remain (unreacted) in the glass

273   (i.e., $X_{BO} = X_{O2-}$). If the amount of unreacted BO is 'x' then the concentration of O^{2-} in the glass

274   is also 'x' and the amount of NBO is the total oxygen in the glass is '$O_T -2x$' where $O_T =$

275    $X_{CaO}+2X_{SiO2}$. Converting to mole fractions and substitution into Eq. (2) yields:

276    $$K_1 \ = \ X_{NBO}{}^2/(X_{BO}X_{O2-}) \ = \ (1-2x)/x^2 \tag{3}$$

277   If, at the orthosilicate composition, *either* X_{BO} *or* X_{O2-} is known, K_1 can be calculated and the

278   concentrations of all oxygen species can be evaluated. These types of calculations were

279   performed on Ca-Mg-silicate glasses to obtain BO, NBO and O^{2-} abundances for numerous

280   experimental studies discussed subsequently. The results are compiled in Table 2.

12

281   **Raman Spectral Results.** Nasikas et al. (2011) reported Raman spectra for of the Ca_1Mg_1-

282   silicate glasses containing 28, 30 and 33 mol% SiO_2 (CMS28, CM30 and CMS33 glasses). They

283   fit the Raman spectrum of the CaMg orthosilicate glass (CMS33) and reported 50% Q^0, 35% Q^1,

284   13% Q^2 and 2% Q^3. From these the NBO, BO and O^{2-} mole fractions were determined and X_{O2-}

285   = 0.084, or 8.4 mol% O^{2-} (for calculations, see Sawyer et al., 2015, their Appendix A). The O

286   species abundances are listed in Table 2. Nasikas et al. (2012) assign an uncertainty of $\pm3\%$ to

287   their Q species abundances. The uncertainty was added to, and subtracted from, Q^1 (with

288   compensation in Q^0) to obtain 8.8% and 8.0% O^{2-} respectively. The uncertainty then was added

289   to, and subtracted from, Q^2 (with compensation in Q^0) to yield respectively 9.1% and 7.6% O^{2-}.

290   The Raman results for the CMS33 sample therefore yields 8.4 (±0.8) mol% O^{2-} which, as shown

291   in Fig. 4a, is remarkably close to the 9.5% O^{2-} value obtained by fitting the CMS33 ^{17}O NMR

292   spectrum of Nasikas et al. (2012).

293   ^{17}O **NMR and Raman Spectra of Ca_1Mg_1-Silicate Glasses.** Nasikas et al. (2012) provide ^{29}Si

294   MAS NMR and ^{17}O MAS NMR spectra of the Ca_1Mg_1-silicate glasses containing 28 and 33

295   mol% SiO_2 (CMS28 and CMS33). They identified the O^{2-} and NBO+BO peaks in their ^{17}O

296   NMR spectra, but they do not fit the spectra and in an attempt at quantification, these spectra

297   were scanned and digitized, imported into and fitted using CASAXPS software. The dots of Fig.

298   4 represent the scanned spectra. After introducing a linear background and two 100% Gaussian

299   peaks to each spectrum, a least squares, entirely free fit was performed (fit parameters given in

300   Table 1). Following Nasikas et al. (2012), the more intense peak was interpreted as the NBO+BO

301   contribution and the weaker peak as O^{2-}. The fits to the CMS33 and CMS28 glasses of Figs 4a

302   and 4b yield respectively ~9.5 mol% and ~19.3 mol% O^{2-}. Nasikas et al. (2012) quoted ~5 mol%

303   O^{2-} for the orthosilicate glass (CMS33) which is somewhat lower than the 8.4 (±0.8) mol% O^{2-}

13

304   obtained from their Raman results discussed in the previous paragraph, and from our fit (Fig. 4a).

305   In fitting the ^{17}O NMR spectra, backgrounds were set to minimize the area of the O^{2-} peak (i.e.,

306   background was set at the highest possible intensity on the high ppm side of the spectra) so that

307   mol% O^{2-} values (~9.5% and ~19.3% O^{2-} for CMS33 and CMS28 respectively) are near

308   minimum values. Other background settings yield greater O^{2-} abundances by 1 to 3 mol%.

309   The NBO and BO contributions cannot be distinguished in the ^{17}O NMR spectra (Figs.

310   4a, 4b) but at the orthosilicate composition the two peaks can be separated using the constraint

311   that $X_{BO} = X_{O2-}$ (see Introduction to this section), in a manner analogous to separation of NBO

312   and O^{2-} peaks in Fig. 2a. Three 100% Gaussian peaks, one representing each of BO, NBO and

313   O^{2-}, were introduced to Fig. 4c. The BO and O^{2-} peak intensities were *constrained* to identical

314   values but their peak widths and positions were unconstrained. The NBO peak parameters were

315   unconstrained. The resulting fit to CMS33 glass is illustrated in Fig. 4c and the residuals are

316   shown in Fig. 4e. Fitted peak parameters are provided in Table 1. The fit is somewhat better than

317   the two peak fit of Fig. 4a and it yields 10.3 mol% for O^{2-} and BO, and 79.4 mol% NBO. The fits

318   to Figs. 4a and 4c indicate that the O^{2-} mol% for the CMS33 glass should be ~10 mol% O^{2-}. Cast

319   as mole fractions and substituted into Eq. (2) yields $K_1 = 59.4$.

320   **Test for Consistency.** A test is performed to determine if the ^{17}O NMR spectra results for the

321   CMS33 and CMS28 are consistent with each other. Peak area constraints were used to obtain the

322   three peak fit to the Pb77 glass (Fig. 2b) and an identical procedure has been used to evaluate

323   oxygen speciation in the CMS28 glass. Three independent equations were used to solve for the

324   mole fractions of the three oxygen species in the CMS28 glass. The equations are the mass

325   action equation with $K_1 = 59.4$ (derived from the CMS33 glass), the stoichiometry of the

326   polymerization reaction (Eq. 1) and the mass balances constraint where $\Sigma X_{O-species} = 1.0$ (see

327   Sawyer et al. 2015 for details). The result is $X_{NBO} = 0.765$, $X_{BO} = 0.055$ and $X_{O2-} = 0.180$ for the

328   CMS28 glass. These were used to calculate $X_{BO}/X_{NBO} = 0.0716$ and $X_{O2-}/X_{NBO} = 0.235$. These

329   ratios then were used to constrain BO/NBO and O^{2-}/NBO peak areas during fitting of the CMS28

330   ^{17}O NMR spectrum. No other constraints were used. The resulting fit is shown in Fig. 4d,

331   residuals in Fig. 4f, and the fit parameters are given in Table 1. Clearly the BO, NBO and O^{2-}

332   peak areas derived from simultaneous solutions of the above three equations are consistent with

333   the ^{17}O NMR spectrum for CMS28, and with $K_1 = 59.4$ for both glasses. The X_{BO} values for the

334   CMS28 and CMS33 glasses are plotted on Fig. 5a as solid diamonds and the corresponding X_{O2-}

335   values are plotted are plotted as crosses (at the same compositions). The ^{17}O NMR spectra of

336   Nasikas et al. (2012) clearly are consistent with each other and with the mass action equation

337   where $K_1 = 59.4$.

338   **Uncertainties.** Different fits to the scanned spectra (Fig. 4) indicate that O^{2-} represents about

339   10 mol% of total oxygen in the orthosilicate glass (Figs. 4a, 4c). Variation in line shapes (i.e.,

340   addition of a Lorentzian component to the peaks) and placement of background indicate ~9.5

341   mole% to ~13 mol% O^{2-} for the CMS33 glass. This variation results solely from fitting the

342   spectra but uncertainty is introduced by scanning the spectra and by assuming that all oxygen

343   peaks contributing to the ^{17}O NMR spectra are symmetric (Gaussian). Considering these, we

344   estimate that the accuracy of our O^{2-} abundances is no better than about ±4 mol% in O^2. We

345   conclude that O^{2-} represents 10 ±4 mol% of total oxygen in CMS33 glass and 18 ±4 mol% in

346   CMS28 (Figs. 4b, 4d).

347   **O^{2-} in Other Ca_1Mg_1-Silicate Glasses.** Schneider et al. (2000) report Q-species abundances

348   from a ^{29}Si MAS NMR spectrum of $Ca_{0.5}Mg_{0.5}SiO_3$ glass and calculation of oxygen species

349   abundances (Table 2) yielded 0.8 mol% O^{2-}. Taking $K_1 = 59.4$ and considering the stoichiometry

350   of Eq. (1) and $\Sigma X_{O\text{-species}}$ = 1.0 (see Sawyer et al. 2015 for details), the percentages of BO, NBO

351   and O^{2-} calculated for this glass are respectively 35.2 mol%, 62.9 mol% and 1.9 mol%; O^{2-} is ~

352   double that obtained from the Q species abundances of Schneider et al. (2000). Their spectrum,

353   however, consisted of one broad, asymmetric peak with no defining shoulders or inflections and

354   the O^{2-} uncertainty associated with the Q species abundances is large. The same calculations

355   were applied to the disilicate glass ($Ca_{0.5}Mg_{0.5}Si_2O_5$) yielding 60.5%, 39.1% and 0.4%

356   respectively for BO, NBO and O^{2-}. No spectra are available for comparison.

$CaO\text{-}SiO_2$ Glasses

$CaSiO_3$ (metasilicate) Glass. Pedone et al. (2010) presented a theoretical treatment of $CaSiO_3$

359   glass. They emphasized that fits to ^{29}Si MAS NMR spectra using Gaussian line shapes do not

360   yield accurate Q-species abundances because some Q-species peaks are non-Gaussian. They

361   noted, however, that Gaussian peak shapes may be used to obtain reasonable Q-species

362   abundances from 2D ^{29}Si NMR spectra of $CaSiO_3$. Zhang et al. (1997) came to a similar

363   conclusion concerning the fitting of ^{29}Si MAS NMR spectra. We therefore focus on the 2D ^{29}Si

364   MAF NMR spectrum of Zhang et al. (1997) which is by far the most comprehensive study of this

365   glass. They list Q-species abundances consistent with their 2D ^{29}Si NMR spectrum (their Table

366   1) and report ~1 mol% O^{2-} in the glass. From their Q species values we calculated BO, NBO and

367   O^{2-} abundances with O^{2-} ~0.9 mol%. Values are listed in Table 2 and are plotted on Fig. 5a (X_{BO}

368   as shaded circles, X_{O2-} as crosses). Zhang et al. (1997) quoted one standard deviation uncertainty

369   (σ) in their Q species abundances and to assess the uncertainty in O^{2-} we applied 2σ to the Q^3

370   and Q^4 abundances, and decreased by 2σ, Q^0 and Q^1 abundances. Q^2 was obtained from the

371   constraint that $\Sigma_{Q\text{-species}}$ = 100. The maximum and minimum O^{2-} values obtained were 1.3 and 0.6

372   mol%. We conclude that O^{2-} = 1.0 ($\pm$0.4) mol%.

16

373   **$Ca_{0.56}Si_{0.44}O_{1.44}$ (CS56) Glass.** Thompson et al. (2012) reported a ^{17}O MAS NMR study of

374    $Ca_{0.56}Si_{0.44}O_{1.44}$ glass (CS56) and used two methods to obtain NBO and BO abundances. The

375   more accurate method (Method#1) yielded 75.4 ±0.6 mol% NBO and 24.6 mol% BO whereas

376   the second (Method#2) yielded 76.9 ±1.2 mol% NBO and 23.1 mol% BO. Had the

377   polymerization reaction (Eq. 1) gone to completion (i.e., $K_1 = \infty$), two NBO atoms would be

378   present for each Ca atom in the glass so that NBO = 78.6 mol% and BO = 21.4 mol% at this

379   composition. By Method#1 or Method#2, BO is in excess of that expected if the reaction went to

380   completion. From the stoichiometry of Eq. (1), the excess in BO must equal the amount of

381   unreacted O^{2-} remaining in the glass; thus by Method#1 there is 3.2 mol% O^{2-} in the glass (24.6 –

382   21.4 = 3.2 mol% excess BO = 3.2 mol% unreacted O^{2-}). By Method#2 the unreacted O^{2-}

383   remaining in the glass is 1.7 mol%. Clearly the de-polymerization reaction (Eq. 1) did not go to

384   completion and there is free oxygen in the glass.

385   Thompson et al. (2012) did not observe a separate O^{2-} peak so that it may reside

386   underneath the NBO peak of the ^{17}O NMR spectrum or elsewhere in the spectrum. If, for

387   example, it resided underneath the BO peak, then the O^{2-} values just calculated represent

388   minimum values. Uncertainty in the composition of the CS56 glass (Thompson et al. 2012) is

389   reflected in the uncertainty of the NBO and BO values (i.e., ±1.4 mol%; Thompson et al. 2012).

390   Considering the uncertainties, O^{2-} is evaluated at 3.2 mol% ±2.0 mol% by the more accurate

391   analytical method and 1.7 mol% ±2.6 mol% by 'Method#2'. These are listed in Table 2. X_{BO} and

392   X_{O2-} were calculated and plotted on Fig. 5a as shaded circles and crosses. The oxygen species

393   abundances are entirely consistent with those of Zhang et al. (1997) and the results conform,

394   within experimental uncertainties, to the mass action equation with $K_1 \sim 60$ as shown in Fig. 5a

395   (solid curves represent O-species abundances for $K_1 = 59.4$). The apparent discrepancy between

17

396   Zhang et al. (1997), who state that O^{2-} is present in $CaSiO_3$ glass, and Thompson et al. (2012),

397   who state there is no evidence for O^{2-} in the 56.6 mol% CaO glass, is resolved by accepting the

398   ^{17}O NMR experimental results for CS56 glass of Thompson et al. (2012). We conclude that there

399   are a few mol% O^{2-} in Ca-silicate glasses ranging in composition from $CaSiO_3$ to Ca_2SiO_4.

400   **MgO-SiO$_2$ Glasses**

401   **Mg$_2$SiO$_4$ Glass (orthosilicate).** Davis et al. (2011) conducted ^{29}Si 2D MAF NMR studies of

402   Mg_2SiO_4 glass and observed Q^1 species which, at this composition, necessarily indicates the

403   presence of BO and O^{2-} in equal amount. From their Q-species proportions (y_{Qn} values of their

404   Table 2) the mol% of NBO, BO and O^{2-} were calculated (Sawyer et al. 2015) to obtain BO = 4.5

405   ± 1 mol%, NBO = 91 ± 2 mol% and O^{2-} = 4.5 ± 1 mol% (Table 2). Sen et al. (2009) also report Q-

406   species distributions for Mg_2SiO_4 glass from a ^{29}Si MAS NMR study and obtained near-identical

407   results (BO:NBO:O^{2-} = 5:90:5, no uncertainties provided). A ^{29}Si static and MAS NMR study by

408   Sen and Tangeman (2008) report that Q^0 = 49 ± 4 mol% and Q^1 = 51 ± 4 mol% in Mg_2SiO_4 glass

409   from which BO:NBO:O^{2-} = 6.4:87.2:6.4 (Table 2). BO and O^{2-} uncertainties were evaluated at

410   ± 0.5 mol%. The three ^{29}Si NMR studies of Mg_2SiO_4 glass yield remarkably consistent results,

411   indicating between 4 and 7 mol% BO and O^{2-} (Table 2, Fig. 5a).

412   **MgSiO$_3$ Glass.** The ^{29}Si NMR studies of Davis et al. (2011) and Sen et al. (2009) provide Q-

413   species abundances for $MgSiO_3$ glass from which O-species abundances were calculated, listed

414   in Table 2 and plotted on Fig. 5a (shaded circles). The Davis et al. (2011) experiment yields 1.0

415   mol% O^{2-} whereas the results of Sen et al. (2009) give 2.6 mol% O^{2-}. Mountjoy et al. (2011) also

416   concluded that there was O^{2-} in $MgSiO_3$ glass based on his fit to a ^{17}O NMR spectrum.

417   Apparently, free oxide (O^{2-}) is present in $MgSiO_3$ glass at about the same level as found in the

418   $CaSiO_3$ glass of Zhang et al. (1997). The mass action equation with K_1 = 59.4 (Eq. 2) yields O^{2-}

18

419   ~ 1.9 mol% for metasilicate glass indicating that free oxide is of the same order in both Ca- and

420   Mg-metasilicate glasses.

421   Allwardt and Stebbins (2004) published a well resolved ^{17}O NMR spectrum of MgSiO$_3$

422   glass. It was left to Mountjoy et al. (2011) to fit the spectrum but they did not include the

423   extremities of the spectrum in their fit and in an attempt to determine details of the relationships

424   among the oxygen species we have scanned and fit the spectrum (Fig. 6). The strongest peak is,

425   according to Allwardt and Stebbins (2004), a NBO peak and like Stebbins and Sen (2013) we

426   use a symmetric Gaussian peak to fit it. Allwardt and Stebbins (2004) note the non-Gaussian

427   (quadrupole) BO lineshape of CaMg and Ca metasilicates and the tail on the right side of Fig. 6

428   suggests a quadrupole lineshape for BO of MgSiO$_3$ glass. Two Gaussian peaks were employed

429   (Fig. 6, BO#1 and BO#2) solely to fit the low frequency part of the spectrum and to obtain the

430   area of the BO contribution (the peaks have no other significance). The broad contribution

431   extending from ~ 70 to ~ 180 ppm was fit with a Gaussian lineshape and is labelled '?'. Its origin

432   is uncertain. Areas (%) of each contribution are provided in Fig. 6 and fit parameters are given in

433   Table 1. An alternative fit to the spectrum would have a linear background extending from -150

434   ppm to about 100 ppm. Such a background would obviate the need to introduce the peak labelled

435   '?'. A least squares fit using this background, the NBO, BO#1 and BO#2 peaks yields, however,

436   NBO and BO peak areas similar to the values shown in Fig. 6.

437   The coordination number of free oxygen (O^{2-}) in Mg-silicate melts and glasses cannot yet

438   be determined with certainty and as a result, neither can its position in the ^{17}O NMR spectrum.

439   The NBO and BO contents, however, can be used to estimate of O^{2-} abundance. Normalizing the

440   BO and NBO peak areas listed in Fig. 6 to 100%, then NBO = 63.4% and BO = 36.6%. If the

441   polymerization reaction (Eq. 1) had gone to completion (all O^{2-} consumed) the BO content

19

442 would be 35.1%, indicating a ~1.5 mol% excess of BO in the glass (i.e., the reaction did not go

443 to completion). By the stoichiometry of the polymerization reaction there is an amount of

444 unreacted O^{2-} in the glass equal to the excess BO (i.e., $O^{2-} \sim 1.5$ mol%). Assuming the 1.5 mol%

445 O^{2-} is under the peak labelled "?" of Fig. 6 (and renormalizing the three O contributions to 100

446 mol%) the proportions of oxygen species (NBO:BO:O^{2-}) ~ 62.4:36.1:1.5.

447   The uncertainty associated with the O^{2-} mol% cannot be readily evaluated because the

448 spectrum was scanned. The value of 1.5 mol% O^{2-} in the MgSiO$_3$ glass is, however, consistent

449 with the results of Davis et al. (2011) and Sen et al. (2009), with all three NMR results indicating

450 1.5 ($\pm$1) mol% O^{2-}. Equally important, *all* eight NMR spectral results for Mg$_2$SiO$_4$ and MgSiO$_3$

451 glasses, and CMS33 and CMS28 glasses, are consistent with the mass action equation (Eq. 2)

452 where $K_1 \sim 60$ (Nasikas et al. 2012; Davis et al. 2011; Sen et al. 2009; Sen and Tangeman, 2008;

453 Allwardt and Stebbins, 2004).

454 **Other Experimental Studies.** Tangeman et al. (2001) report Q^1 species in the ^{29}Si MAS NMR

455 spectrum of Mg$_2$SiO$_4$ glass but do not provide Q-species abundances. Nevertheless, the

456 identification of Q^1 species for this glass composition requires the presence of O^{2-}. Kohara et al.

457 (2004) conducted X-ray and neutron scattering on Mg$_2$SiO$_4$ glass which revealed MgO$_4$, MgO$_5$

458 and MgO$_6$ polyhedra. Some oxygen atoms bridge only the polyhedra making them O^{2-} using our

459 nomenclature. Kohara et al. (2011) used Reverse Monte Carlo fits to diffraction data and density

460 functional theory to model MgSiO$_3$ and Mg$_2$SiO$_4$ glasses and again concluded that MgO

461 polyhedra existed in these glasses. The three studies require O^{2-} to be present and indicate that K_1

462 is finite. The conclusions are also consistent with MD simulations as now discussed.

463   **EVIDENCE FOR FREE OXIDE FROM MD SIMULATIONS**

464   Molecular Dynamics (MD) simulations on Ca and Mg silicate systems discussed below

20

465 indicate mol% levels of O^{2-} in Ca, Mg and CaMg silicate glasses. There are 9 metasilicate, 4

466 orthosilicate MD simulations, and 3 simulations of compositions intermediate between

467 metasilicate and orthosilicate glass, for a total of 16 simulations. All indicate the presence of O^{2-}.

468 In this regard, MD simulations, O 1s XPS, NMR and Raman results are remarkably consistent.

469 The oxygen species abundances derived from these studies are collated and presented in Table 3,

470 and X_{BO} and X_{O2-} values are plotted on Fig. 5b.

471 **CaMg-Silicate Glasses**

472 Al-Hasni and Mountjoy (2014) reported MD simulations of glasses ranging in

473 composition from $MgSiO_3$ (metasilicate) to Mg_2SiO_4 (orthosilicate). They report Q-species

474 abundances and from these the O-species abundances were calculated, tabulated (Table 3) and

475 plotted on Fig. 5b. All plot above the curve where $K_1 = \infty$ indicating that free oxygen is present

476 at all compositions although in somewhat greater concentrations than obtained from the ^{17}O

477 NMR results (Fig. 5a, diamonds). Mead and Mountjoy (2006), Mountjoy et al. (2011) and Al-

478 Hasni and Mountjoy (2014) emphasize that simulated quench rates are much greater than

479 experimental rates ($\sim 10^{10}$ times). If the structure has not completely adjusted to the quenched

480 temperatures, the distribution of species (e.g., Q species and O species) may retain residual

481 distributions reflective of a greater temperature. To summarize, the MD studies may apply to

482 temperature conditions different from those of the ^{17}O NMR study (Nasikas et al. 2012). If this

483 situation holds one must conclude that O^{2-} is present in the glasses and that it is more abundant in

484 melts (high temperature) than in glasses at ambient temperature.

485 MD simulations on Ca-Mg metasilicate glasses by Cormier and Cuello (2013) include

486 four glasses containing $\sim$ 50 mol% SiO_2, but they have differing proportions of CaO and MgO.

487 They list BO, NBO and O^{2-} mol% in their Fig. 9 and these have been extracted, tabulated (Table

21

488   3) and plotted on Fig. 5b. All contain free oxide and are consistent with the results of Al-Hasni

489   and Mountjoy (2014). MD simulations indicate that O^{2-} is present at mol% levels in invert

490   MgCa-silicate glasses. Secondly, K_1 is finite in this ternary system so that the three oxygen

491   species must exist at all compositions within the system. We emphasize, however, that O^{2-}

492   should be very low in all highly siliceous glasses, and perhaps beyond the detectability.

Mg-Silicate Glasses

494   Ghosh et al. (2014) conducted MD simulations on $MgSiO_3$ glass from which they list Q

495   species abundances. The Q species distribution of their lowest pressure simulation yields O^{2-} of

496   ~3.4 mol% (Table 3). Mountjoy et al. (2011) conducted an MD simulation of $MgSiO_3$ and

497   reported that it contained ~4.5 mol% O^{2-} in the glass, which compares favourably with the result

498   of Ghosh et al. (2014). They did not, however, report BO and NBO abundances nor Q species

499   abundances so that BO and NBO abundances are not recorded in Table 3.

500   Spiekermann et al. (2013) conducted MD simulations of Mg_2SiO_4, $MgSiO_3$ and $MgSi_2O_5$

501   glasses. They quoted Q-species abundances and from these the oxygen species concentrations

502   were determined and listed in Table 3. O^{2-} was present at 7.8 mol% in Mg_2SiO_4 glass, at 4.8

503   mol% in $MgSiO_3$ glass and 0.8 mol% O^{2-} was present in $MgSi_2O_5$ glass. These free oxygen

504   abundances are commensurate with O^{2-} concentrations in the CaMg-silicate glasses of Al-Hasni

505   and Mountjoy (2014).

506   Sen and Tangeman (2008) and de Koker et al. (2009) report MD simulations of Mg_2SiO_4

507   glass and melt, and they provide Q-species abundances. The Sen and Tangeman (2008) result

508   gives 5 mol% O^{2-} for Mg_2SiO_4 glass and de Koker et al. (2009) yields 15 mol% for the same

509   glass composition (Table 3). These results straddle X_{BO} curve for $K_1 = 59.4$ on Fig. 5b. The de

510   Koker et al. (2009) result (Table 3) is almost identical to the Mg_2SiO_4 result of Al-Hasani and

22

511 Mountjoy (2014) and the Sen and Tangeman (2008) result is similar to the Mg_2SiO_4 of

512 Spiekermann et al. (2013). These MD simulations are remarkably consistent with respect to O^{2-}

513 abundances in glasses ranging in composition from the disilicate ($MgSi_2O_5$) to Mg_2SiO_4.

514 **Ca-silicate Glasses**

515 Mead and Mountjoy (2006) and Cormier and Cuello (2013) provide MD simulations of

516 Ca-metasilicate glass. The former study reports Q-species abundances where $Q^0:Q^1Q^2:Q^3:Q^4 =$

517 6:23:40:25:8. From these values the O species abundances were calculated and are listed in

518 Table 3. Cormier and Cuello (2013) plot Q species abundances and from the plot $Q^0:Q^1Q^2:Q^3:Q^4$

519 ~ 5:24:36:28:7. They also plot oxygen species abundances in their Fig. 9 and these have been

520 extracted and included in Table 3, and plotted on Fig. 5b. The Mead and Mountjoy (2006) result

521 indicates 1.0 mol% O^{2-} in the glass whereas the Cormier and Cuello (2013) result yields 1.3

522 mol% O^{2-}. These results agree with the 2D ^{29}Si MAF NMR experimental result (Zhang et al.

523 1997) which gives 1.0 (±0.4) mol% O^{2-}. Wu et al. (2015) conducted MD simulations on the

524 $CaO-SiO_2$ system. They plotted their oxygen species on diagrams and these have been extracted

525 and included in Table 3 and plotted on Fig. 5b. The O^{2-} values are similar to those of Al-hasni

526 and Mountjoy (2014) for the Mg-silicate system. Pedone et al. (2010) determine Q species

527 abundances for $CaSiO_3$ glass using approaches different from the above two MD studies. One

528 model indicates minor O^{2-} with $Q^0:Q^1Q^2:Q^3:Q^4$ ~ 0:23:53:17:7 and the second yields

529 $Q^0:Q^1Q^2:Q^3:Q^4$ ~ 0:27:50:20:3 but these give a physically impossible BO value (Fig. 6) and a

530 negative O^{2-} value.

531 A ^{29}Si MAS NMR spectrum for $CaSiO_3$ glass redrawn after Zhang et al. (1997) is

532 reproduced in Fig. 7a along with their free fit to the spectrum. Zhang et al. (1997) emphasize that

533 the fit to Fig. 7a is incorrect in that Q^2 is too abundant and Q^0, Q^1 and Q^4 are absent. They

534   obtained more accurate Q species values by projecting their 2D ^{29}Si MAF NMR spectrum onto

535   the MAS dimension and fitting Q species signals to the projected spectrum using constraints

536   derived from the 2D ^{29}Si MAF NMR spectrum. The projected spectrum and fit are illustrated in

537   Fig. 7b. The Q species distributions of Mead and Mountjoy (2006), Cormier and Cuello (2013)

538   and Pendone et al. (2010) agree better with the Q species distribution of Fig 7b than with that of

539   Fig. 7a. Accepting the fit in Fig. 7b, we conclude that Q species distributions derived from the

540   simulations are as accurate as Q species abundances derived from a *free fit* to the ^{29}Si MAS

541   NMR spectrum of $CaSiO_3$ glass. The Q^2 peak, for example (Fig. 7a) is very broad, primarily

542   because there is no spectral feature to constrain its width. Poor spectral resolution (i.e., no strong

543   shoulders or minima) precludes extraction of accurate Q species abundances from Fig. 7a or

544   from any similarly resolved spectrum.

Implications

546   The high resolution of the new generation of XPS instrument has been used to detect, and

547   for the first time to accurately quantify the amount, of O^{2-} (free oxygen) in binary silicate Pb

548   glasses. The advance results primarily from a technical development whereby surface charging

549   of insulators (e.g., silicate glasses) is effectively eliminated. This, coupled with detailed

550   knowledge of O 1s XPS lineshapes and linewidths, allows for accurate measurement of oxygen

551   species in binary glasses (e.g., Sawyer et al., 2015; 2012; Nesbitt et al., 2011). Once measured at

552   one composition, the equilibrium constant for Eq. 2 allows calculation of oxygen species

553   abundances in more siliceous glasses. The mass action equation relating the three oxygen species

554   (Eq. 2) necessarily holds across the *entire* binary silicate system, requiring all three species to be

555   present in all binary melts where equilibrium is established. Most emphatically, O^{2-} is an

556   essential, thermodynamically important constituent of binary Pb, Ca and Mg silicate melts and

24

557 glasses. Clearly, O^{2-} obtained in MD simulations is *not* just an 'accidental product' associated

558 with (rapid) cooling rates employed in the simulations (Cormier and Cuello, 2013).

559   Determination of O species abundances in silicate melts has exceedingly important

560 implications concerning the reactivity of glasses. Of the three oxygen species O^{2-} is by far the

561 most basic and will be much more reactive toward H_2O, CO_2 and sulfur gases than will be BO or

562 NBO (Sawyer et al., 2015). There is also a large supply of O^{2-} in melts. Any O^{2-} consumed by

563 reaction will be replenished via reaction (1) according to the principle of Le Chatelier. Reaction

564 (1) acts like a classic buffer maintaining near-constant O^{2-} abundances in melts during reaction.

565 The buffer capacity of the reaction may be exceedingly large and is dependent primarily on the

566 NBO content of the melt or glass. As a result, even low concentrations of O^{2-} may control

567 reaction rates due to its continual replenishment.

568   Accurate quantification of O 1s XPS, 2D ^{17}O NMR spectra and 2D ^{29}Si NMR spectra

569 now can be achieved (e.g., Fig. 1; Davis et al., 2010; Florian et al., 1996; Farnan et al., 1992).

570 Interpretation and quantification of many published spectra, however, are very difficult because

571 spectra are poorly resolved, or lineshapes and linewidths are uncertain with spectral properties

572 varying according to experimental conditions and glass compositions. As a result of these

573 problems, many ^{17}O NMR, ^{29}Si MAS NMR and XPS O 1s spectra have been published with no

574 fits (or only partial fits) yet species abundances have been quoted based on the spectra.

575 Unfortunately, without complete fits, quoted abundances of species cannot be tested or verified

576 and must be questioned. Here, we have attempted to show how detailed, complete fitting of

577 spectra, combined with the use of mass and charge balances, can be used to extract species

578 abundances from complex spectra, and to assign realistic uncertainties to the abundances.

579   **CONCLUSIONS**

25

580   There is direct O 1s XPS experimental evidence for ~35 mol% O^{2-} in the Pb-silicate glass

581   containing 76.6 mol% PbO. This amount is consistent with the ^{29}Si MAS NMR and O 1s XPS

582   results for the binary, and with the mass action equation where K_1 ~12. There is also direct ^{17}O

583   NMR experimental evidence for ~ 10 mol% O^{2-} in CaMg-orthosilicate glass (Nasikas et al.

584   2012). 2D ^{29}Si MAF NMR spectral evidence demonstrates ~ 1 mol% O^{2-} in Ca-metasilicate glass

585   (Zhang et al. 1997) and the ^{17}O NMR result a glass containing 56.6 mol% CaO yields ~3 mol%

586   O^{2-} (Thompson et al. 2012).   Eight separate NMR results for Mg-silicate glasses indicate ~1

587   mol% O^{2-} in $MgSiO_3$ glass and ~5 mol% or more in Mg_2SiO_4 glass (Table 2). Importantly the

588   CaMg silicate, Ca silicate and Mg-silicate glasses are thermodynamically consistent indicating

589   that K_1 ~ 60 with uncertainties considered. Many MD calculations pertaining to Mg-silicate

590   glasses CaMg-silicate glasses have indicated O^{2-} at the 0.5 to 15 mol% range (Table 3). From

591   these results we conclude that free oxide is present in the binary $CaO-SiO_2$, $MgO-SiO_2$ and likely

592   is present in ternary $CaO-MgO-SiO_2$ glasses and melts. The most reliable ^{29}Si NMR studies are

593   the 2-D ^{29}Si NMR type (e.g., Davis et al. 2011; 2010; Zhang et al. 1997; 1996).

ACKNOWLEDGEMENTS

599

References

601   Al-Hasni, B.M., and Mountjoy G. (2014) A molecular dynamics study of the atomic structure of

602         $_x(MgO)_{100-x}(SiO_2)$. Journal Non-Crystalline Solids, 389, 33–44.

26

603   Allwardt, J.R., and Stebbins, J.F. (2004) Ca-Mg and K-Mg mixing around non-bridging O atoms

604   in silicate glasses: An investigation using ^{17}O MAS and 3QMAS NMR. American

605   Mineralogist, 89, 777-784.

606   Bancroft G.M., Nesbitt H.W., Ho R., Shaw D.M., Tse J.S., and Biesinger M.C. (2009) Toward a

607   comprehensive understanding of solid state core-level XPS linewidths: experimental and

608   theoretical studies on the Si 2p and O 1s linewidths in silicates. Physical Review B

609   80,075405.

610   Cormier, L., and Cuello, G.J. (2013) Ca and Na environments in $Na_2O–CaO–Al_2O_3–SiO_2$

611   glasses: influence of cation mixing and cation-network interactions. Geochimica et

612   Cosmochimica Acta, 122, 498-510. doi.org/10.1016/ j.gca.2013.04.026.

613   Dalby, K.N., Nesbitt, H.W., Zakaznova-Herzog, V.P., and King, P.L. (2007) Resolution of

614   bridging oxygen signals from O 1s spectra of silicate glasses using XPS: Implications for

615   O and Si speciation. Geochimica et Cosmochimica Acta, 71, 4297–4313.

616   Davis, M.C., Kaseman, D.C., Parvani, S.M., Sanders, K.J., Grandinetti, P.J., Massiot, D., and

617   Florian, P. (2010) $Q^{(n)}$ Species Distribution in $K_2O·2SiO_2$ Glass by ^{29}Si Magic Angle

618   Flipping NMR. Journal of Physical Chemistry A, 114, 5503-5508.

619   Davis, M.C., Sanders, K.J., Grandinetti, P.J., Gaudio, S.J., and Sabyasachi, S. (2011) Structural

620   investigations of magnesium silicate glasses by ^{29}Si 2D Magic-Angle Flipping NMR.

621   Journal of Non-Crystalline Solids, 357, 2787-2795.

622   de Koker, N.P., Stixrude, L., and Karki, B.B. (2009) Thermodynamics, structure, dynamics, and

623   freezing of Mg_2SiO_4 liquid at high pressure. Geochimica et Cosmochimica Acta, 72,

624   1427-1441.

625   Du, J., and Cormack, A.N. (2004) The medium range structure of sodium silicate glasses: a

27

626   molecular dynamics simulation. Journal of Non-Crystalline Solids, 349, 66–79.

627   Farnan, I., Grandinetti, P.J., Baltisberger, J.H., Stebbins, J.F., Werner, U., Eastman, M.A., and

628   Pines, A. (1992) Quantification of the disorder in Network-modified silicate glasses.

629   Nature, 38, 31-35.

630   Fayon, F., Bessada, C., Massiot, D., Farnan, I., and Coutures, J.P. (1998) ^{29}Si and ^{207}Pb NMR

631   study of local order in lead silicate glasses. Journal of Non-Crystalline Solids, 232-234,

632   403-408.

633   Fincham, C.F.B., and Richardson, F.D. (1954) The Behaviour of Sulphur in Silicate and

634   Aluminate Melts. Proceedings of the Royal Society of London, A223, 40-62.

635   Florian, P., Vermillion, K.E., Grandinetti, P.J., Farnan, I., and Stebbins, J.F. (1996) Cation

636   Distribution in Mixed Alkali Disilicate Glasses. Journal of American Chemical Society,

637   118, 3493-3497.

638   Furukawa, T., Brawer, S.A., and White, W.B. (1978) The structure of lead silicate glasses

639   determined by vibrational spectroscopy. Journal of Materials Science, 13, 268-282.

640   Ghosh, D.P., Karki, B.B., and Stixrude, L. (2014) First-principles molecular dynamics

641   simulations of MgSiO3 glass: Structure, density, and elasticity at high pressure. American

642   Mineralogist, 99, 1304-1314.

643   Henderson, G.S. (2005) The structure of silicate melts: a glass perspective. Canadian

644   Mineralogist, 43, 1921-1958.

645   Henderson, G.S., Calas, G., and Stebbins J.F. (2006) The structure of silicate glasses and melts.

646   Elements, 2, 269-273.

647   Iwamoto, N., Tsunawaki, Y., and Miyago, M. (1979) Structural Study of $PbO-SiO_2$ Slags by

648   Raman Spectroscopy. Journal of Japanese Institute of Metals, 43, 1138-1144.

649   Kohara, S., Suzuya, K., Takeuchi, K., Loong, C.-K., Grimstditch, M., Weber, J.K.R., Tangeman,

650   A., and Key, S. (2004) Glass Formation at the Limit of Insufficient Network Formers.

651   Science, 303, 1649- 1652.

652   Kohara, S., Akola, J., Morita, H., Suzuya, K., Weber, J.K.R., Wilding, M.C., and Benmore, C.J.

653   (2011) Relationship between topological order and glass forming ability in densely

654   packed enstatite and forsterite composition glasses. Proceedings of the National Academy

655   of Sciences, 108, 14780-14785.

656   Lee, S.K., and Kim, E.J. (2015) Probing metal-bridging oxygen and configurational disorder in

657   amorphous lead silicate: insights from ^{17}O solid-state nuclear magnetic resonance.

658   Physical Chemistry C, 119, 748-756.

659   Mead, R.N., and Mountjoy, G. (2006) A Molecular Dynamics Study of the Atomic Structure of

660         $(CaO)x(SiO_2)1-x$ Glasses. Journal of Physical Chemistry B, 110, 14273-14278.

661   Mountjoy, G. (2007) The local atomic environment of oxygen in silicate glasses from molecular

662   dynamics. Journal of Non-Crystalline Solids. 353, 1849–1853.

663   Mountjoy, G., Al-Hasni, B.M., and Storey, C. (2011) Structural organisation in oxide glasses

664   from molecular dynamics modelling. Journal of Non-Crystalline Solids. 357, 2522–2529.

665   Mysen, B.O. (2003) Physics and Chemistry of silicate glasses and melts. European Journal of

666   Mineralogy, **15**, 781-802.

667   Nasikas, N.K., Chrissanthopoulos, A., Bouropoulos, N., Sen, S., and Papatheodorou (2011)

668   Silicate Glasses at the Ionic Limit: Alkaline-Earth Sub-Orthosilicates. Chemistry of

669   Materials, 23, 3692–3697.

29

670   Nasikas, N.K., Edwards, T.G., Sen, S., and Papatheodorou, G.N. (2012) Structural

671   Characteristics of Novel Ca−Mg Orthosilicate and Suborthosilicate Glasses: Results from

672   29Si and 17O NMR Spectroscopy. Journal of Physical Chemistry B, 116, 2696-2702.

673   Nesbitt, H.W., Bancroft, G.M., Davidson, R., McIntyre, N,S., and Pratt, A.R. (2004) Minimum

674   XPS core-level line widths of insulators, including silicate minerals. American

675   Mineralogist, 89, 878-882.

676   Nesbitt, H.W., Bancroft, G.M., Henderson, G.S., Ho, R., Dalby, K.N., Huang, Y., and Yan, Z.

677   (2011) Bridging, non-bridging and free (O^{2-}) oxygen in Na_2O-SiO_2 glasses: An X-ray

678   Photoelectron Spectroscopic (XPS) and Nuclear Magnetic Resonance (NMR) study,

679   Journal of Non-Crystalline Solids, 357, 170-180.

680   Nesbitt, H.W., and Bancroft, G.M. (2014) High Resolution Core- and Valence-Level XPS

681   Studies of the Properties (Structural, Chemical and Bonding) of Silicate Minerals and

682   Glasses. Reviews in Mineralogy and Geochemistry, Geological Society of America, 78,

683   271-329.

684   Nesbitt, H.W., Bancroft, G.M., Thibault, Y., Sawyer, R., and Secco, R.A. (2015a) Aspects

685   concerning spectroscopic studies of oxygen speciation in potassium silicate glasses and

686   melts. Canadian Journal of Chemistry, in press.

687   Nesbitt, H.W., Henderson, G.S., Bancroft, G.M., and Ho, R. (2015b) Experimental evidence for

688   Na coordination to bridging oxygen in Na-silicate glasses: Implications for spectroscopic

689   studies and for the modified random network model. Journal of Non-Crystalline Solids,

690   409, 139–148.

691   Park, J.H., and Rhee, P.C-H. (2001) Ionic properties of oxygen in slag. Journal of Non-

692   Crystalline Solids, 282, 7-14.

693   Pedone, A., Charpentier, T., and Menziani, M.C. (2010) Multinuclear NMR of $CaSiO_3$ glass:

694   simulation from first-principles. Physical Chemistry and Chemical Physics, 12, 6054–

695   6066.

696   Retsinas, A., Kalampounias, A.G., and Papatheodorou, G.N. (2014) Reaching the ionic limit in

697   the (1-X)[$Ca_{0.5}$-$Mg_{0.5}$]O–$XSiO_2$ pseudo binary glass system with 0.5 < X < 0.27: Glass

698   formation and structure. Journal of Non-Crystalline Solids. 383, 38-43.

699   Rybicki, J., Rybicka, A., Witkowska, A., Bergmanski, G., Di Cicco, A., Minicucci, M., and

700   Mancini, G. (2001) The structure of lead-silicate glasses: molecular dynamics and

701   EXAFS studies. Journal of Physics of Condensed Matter, 13, 9781-9797.

702   Sawyer, R., Nesbitt, H.W., and Secco, R.A. (2012) Three types of oxygen in K_2O-SiO_2 glasses:

703   an X-ray photoelectron spectroscopy (XPS) study. Journal of Non-Crystalline Solids 358,

704   290-302.

705   Sawyer, R., Nesbitt, H.W., Bancroft, G.M., Thibault, Y., and Secco, R.A. (2015) Spectroscopic

706   Studies of Oxygen Speciation in K-silicate Glasses and Melts. Canadian Journal of

707   Chemistry, 93, 60-73.

708   Schneider, J., Mastelaro, V.R., Panepucci, H., and Zanotto, E.D. (2000) ^{29}Si MAS-NMR studies

709   of Q^n structural units in metasilicate glasses and their nucleating ability. Journal of Non-

710   Crystalline Solids, 273, 8-18.

711   Sen, S., and Tangeman, J. (2008) Evidence for anomalously large degree of polymerization in

712   Mg_2SiO_4 glass and melt. American Mineralogist, 93, 946-949.

713   Sen, S., Maekawa, H., and Papatheodorou, G.N. (2009) Short-range structure of invert glasses

714   along the pseudo-binary join $MgSiO_3$-Mg_2SiO_4: results from ^{29}Si and ^{25}Mg NMR

715   spectroscopy. Journal of Physical Chemistry, 113, 15243-15248.

31

716   Shirley D.A. (1972)   High resolution x-ray photoemission spectrum of the valence bands of Au.

717   Physical Review B 5, 4709-4714.

718   Smets, B.M.J., and Lommen, T.P.A. (1982) The structure of glasses and crystalline compounds

719   in the system PbO-SiO$_2$, studied by x-ray photoelectron spectroscopy. Journal of Non-

720   Crystalline Solids, 48, 423-430.

721   Spiekermann, G., Steele-MacInnis, M., Kowalski, P.M., Schmidt, C., and Jahn, S. (2013)

722   Vibrational properties of silica species in MgO–SiO$_2$ glasses obtained from ab initio

723   molecular dynamics. Chemical Geology, 346, 22-33.

724   Stebbins, J.F. (1995) Dynamics and structure of silicate and oxide melts: nuclear magnetic

725   resonance studies. *In* Structure, Dynamics, and Properties of Silicate Melts (J.F. Stebbins,

726   P.F. McMillan & D.B. Dingwell, eds.). *Reviews in Mineralogy,* **32**, 141-245.

727   Stebbins, J.F., and Sen, S. (2013) Oxide ion speciation in potassium silicate glasses: New limits

728   from ^{17}O NMR. Journal of Non-Crystalline Solids, 368, 17–22

729   Takaishi, T., Takahasi, M., Jin, J., Uchino, T., and Yoko, T. (2005) Structural Study on PbO–

730   SiO$_2$ Glasses by X-Ray and Neutron Diffraction and ^{29}Si MAS NMR Measurements.

731   Journal of American Ceramics Society, 88, 1591–1596.

732   Tangeman, J.A., Phillips, B.L., Navrotsky, A., Weber, J.K.R., Hixson, A.D., and Key, T.S.

733   (2001) Vitreous forsterite (Mg$_2$SiO$_4$): Synthesis, structure, and thermochemistry.

734   Geophysical Research Letters, 28, 2517-2520.

735   Thompson, L.M., McCarty, R.J., and Stebbins, J.F. (2012) Estimating accuracy of ^{17}O NMR

736   measurements in oxide glasses: Constraints and evidence from crystalline and glassy

737   calcium and barium silicates. Journal of Non-Crystalline Solids, 358, 2999-3006.

738   Toop, G.W., and Samis, C.S. (1962) Activities of ions in silicate melts. Transactions of the

739   Metallurgical Society of AIME, 224, 878-887.

740   Wu, T., He, S., Liang, Y., and Wang, Q. (2015) Molecular dynamics simulation of the structure

741   and properties for the CaO–SiO$_2$ and CaO–Al$_2$O$_3$ systems. Journal of Non-Crystalline

742   Solids, 411, 145–151

743   Zakaznova-Herzog, V.P., Nesbitt, H.W., Bancroft, G.M., Tse, J.S., Gao, X., and Skinner, W.

744   (2005) High-resolution valence-band XPS spectra of the nonconductors quartz and

745   olivine. Physical Review B 72, 205113-1 – 205113-13.

746   Zakaznova-Herzog, V.P., Nesbitt, H.W., Bancroft, G.M., and Tse, J.S. (2006) High resolution

747   core and valence band XPS spectra of non-conductor pyroxenes. Surface Science, 600,

748   3175-3186.

749   Zakaznova-Herzog, V.P., Nesbitt, H.W., Bancroft, G.M., and Tse, J.S. (2008) Characterization

750   of leached layers on olivine and pyroxenes using high-resolution XPS and density

751   functional calculations. Geochimica et Cosmochimica Acta, 72, 69–86

752   Zhang, P., Dunlap, C., Florian, P., Grandinetti, P.J., Farnan, I., and Stebbins, J.F. (1996) Silicon

753   site distributions in alkali silicate glass derived by two-dimensional ^{29}Si nuclear magnetic

754   resonance. Journal of Non-crystalline Solids, 204, 294-300.

755   Zhang, P., Grandinetti, P.J., and Stebbins, J.F. (1997) Anionic Species Determination in CaSiO$_3$

756   Glass Using Two-Dimensional ^{29}Si NMR, Journal of Physical Chemistry B, 101, 4004-

757   4008

758

759   **Figure Captions**

760   Fig. 1: O 1s XPS spectra of Pb-silicate glass containing 50 mol% PbO (Fig. 1a), 67 mol% PbO

33

761   (Fig. 1b) and 77 mol% PbO (Fig. lc). The shaded dots represent the experimental data,

762   the thin curves represent the fitted peaks and the background, and the thicker curve

763   represents the fit to the data. The data of Figs. 1a and 1b are taken from Dalby et. al.

764   (2007).

765   Fig. 2: Illustrates two 3-peak fits to the O 1s XPS spectrum of Pb77 glass (76.6 mol% PbO)

766   using different constraints to fit an O^{2-} peak to the spectrum. (a) represents a fit where the

767   FWHM of the BO and NBO peaks were constrained to 1.22 eV and the third peak was

768   unconstrained. (b) represents a fit where the FWHM of the BO peak was constrained to

769   1.22 eV and the proportions of the BO, NBO and O^{2-} peaks were constrained to

770   10.8:54.2:35.0 which are the ratios derived from the fit to Fig. 1c (see text for explanation

771   and Sawyer et al. 2014 for the calculation of O-species abundances).

772   Fig. 3: Illustrates the BO and O^{2-} abundances from experimental results. BO and O^{2-} mole

773   fractions (large and small shaded squares respectively) were calculated from the Q-

774   species abundances obtained from the ^{29}Si MAS NMR results of Fayon et al. (1998). The

775   The large and small shaded circles represent respectively BO and O^{2-} mole fractions

776   calculated from the O 1s XPS results (Dalby et al. 2007). The large and small dots

777   represent respectively the BO and O^{2-} mole fractions obtained by fitting the spectrum of

778   the Pb77 glass (Fig. 1c) and the error bars illustrate the compositional uncertainty. The

779   uncertainty in X_{BO} and X_{O2-} is ±0.02. The thick solid curve illustrates X_{BO} calculated

780   from Eq. (2) with K_1 = 12.0. The dotted, dashed and dash-dot curves represent

781   respectively X_{BO}, X_{NBO} and X_{O2-} calculated for K_1 = infinity (i.e., the polymerization

782   reaction goes to completion).

783   Fig. 4: Fits to the ^{17}O NMR spectra for the Ca_1Mg_1-silicate glasses containing 28 and 33 mol%

34

784   SiO_2 (respectively CMS28 and CMS33 glasses) of Nasikas et al. (2012). (a) and (b)

785   represent two-peak fits to the CMS33 and CMS28 glasses. (c) and (d) represent three

786   peak fits to the same glasses using the same method employed to fit the Pb77 glass of

787   Fig. 2b. (e) and (f) represent the residuals to (c) and (d). The dotted curves represent the

788   spectra published by Nasikas et al. (2012). They were scanned and fitted to quantify these

789   important spectra because no fits were provided in the original publication.

790   Fig. 5: Illustrates oxygen species abundances as a function of composition (mole fraction of MO

791   where MO = MgO, CaO, or CaO+MgO). (a) All data were obtained from experimental

792   studies (see text for sources). All data plot above the dashed curve labelled $K_1 = \infty$. (b) all

793   data were obtained from MD calculations (see text for sources). The solid curves

794   represent the mole fractions of BO, NBO and O^{2-} calculated for K_1 = 59.4 (see Eq. 2).

795   The dashed curves represent the mole fractions of the same species calculated for K_1 =

796   infinity. The shaded areas represent physically impossible values for X_{BO}.

797   Fig. 6: Fit to the ^{17}O NMR spectrum of $MgSiO_3$ glass. The dots represent the scanned spectrum

798   (after Allwardt and Stebbins, 2004) and the curve intersecting the dots is the overall fit to

799   the spectrum. The origin of the peak labelled '?' is uncertain but likely represents a

800   spinning sideband and perhaps O^{2-}. The total BO contribution (solid curve) is asymmetric

801   and is the sum of peaks BO#1 and BO#2. These two BO peaks have no significance other

802   than to allow an estimate of the total BO contribution to the spectrum.

803   Fig. 7: (a) ^{29}Si MAS NMR spectrum of $CaSiO_3$ glass (solid thick curve) and free fit to the

804   spectrum (redrawn after Zhang et al. 1997, their Fig. 5). The dashed curves represent the

805   freely fit curve for each Q species. (b) Projection of the total intensity onto the isotropic

806   dimension and fit after Zhang et al. (1997; their Fig. 4). The solid thick curve respesents

807   the MAS spectrum shown in Fig. 7a and the dashed curves represent the Q species with

808   each lineshape determined from the 2D ^{29}Si MAF NMR spectrum (Zhang et al. 1997,
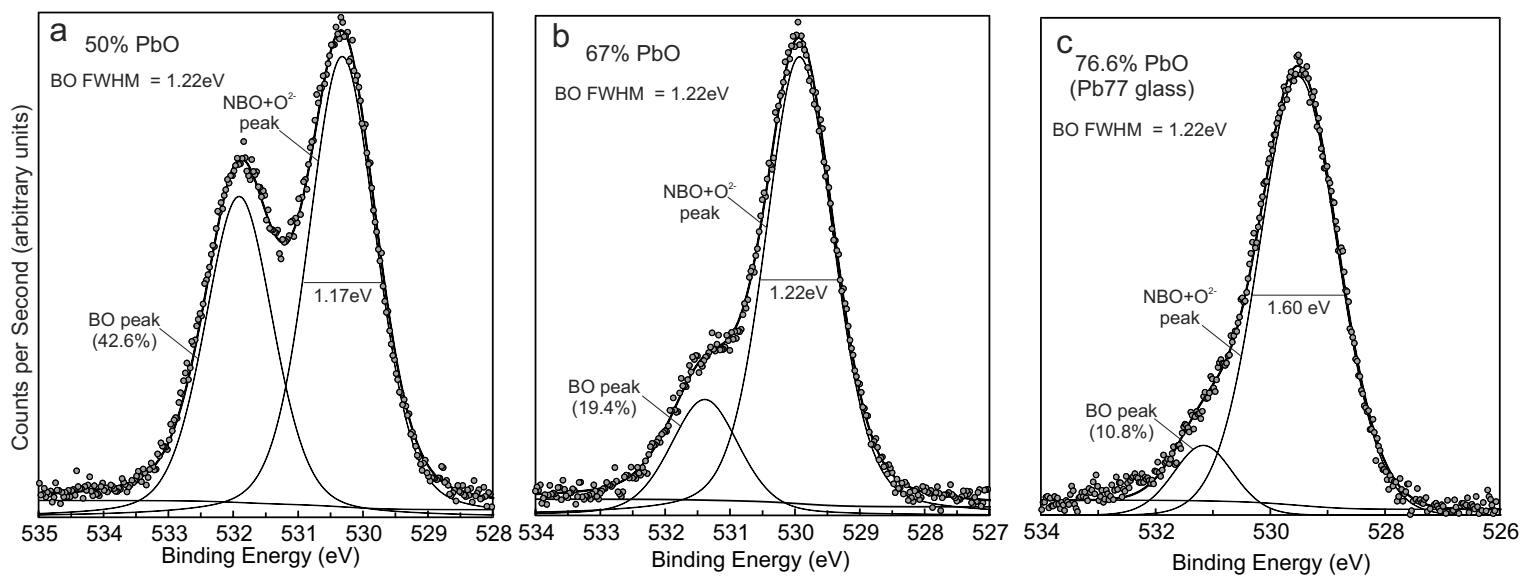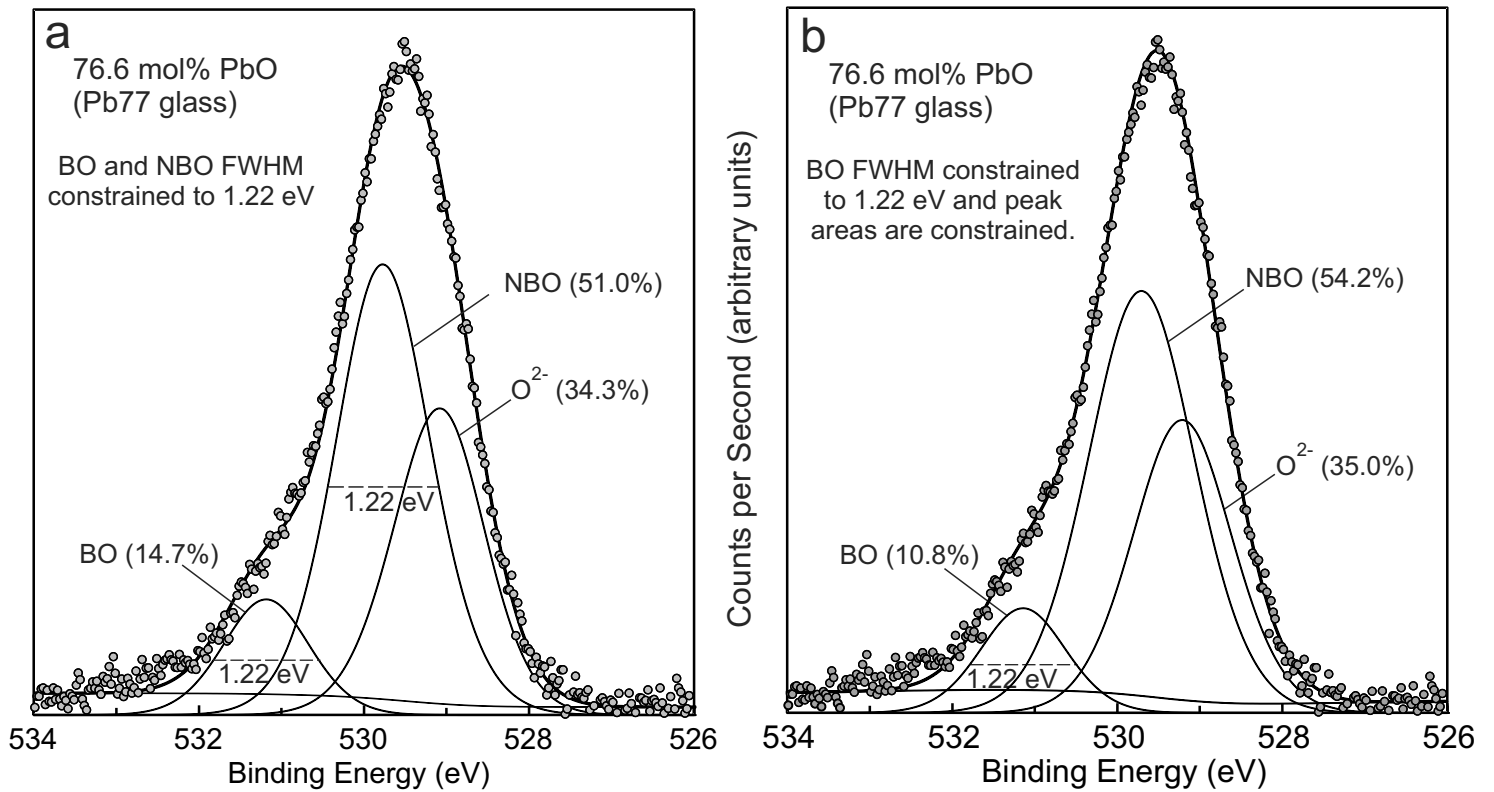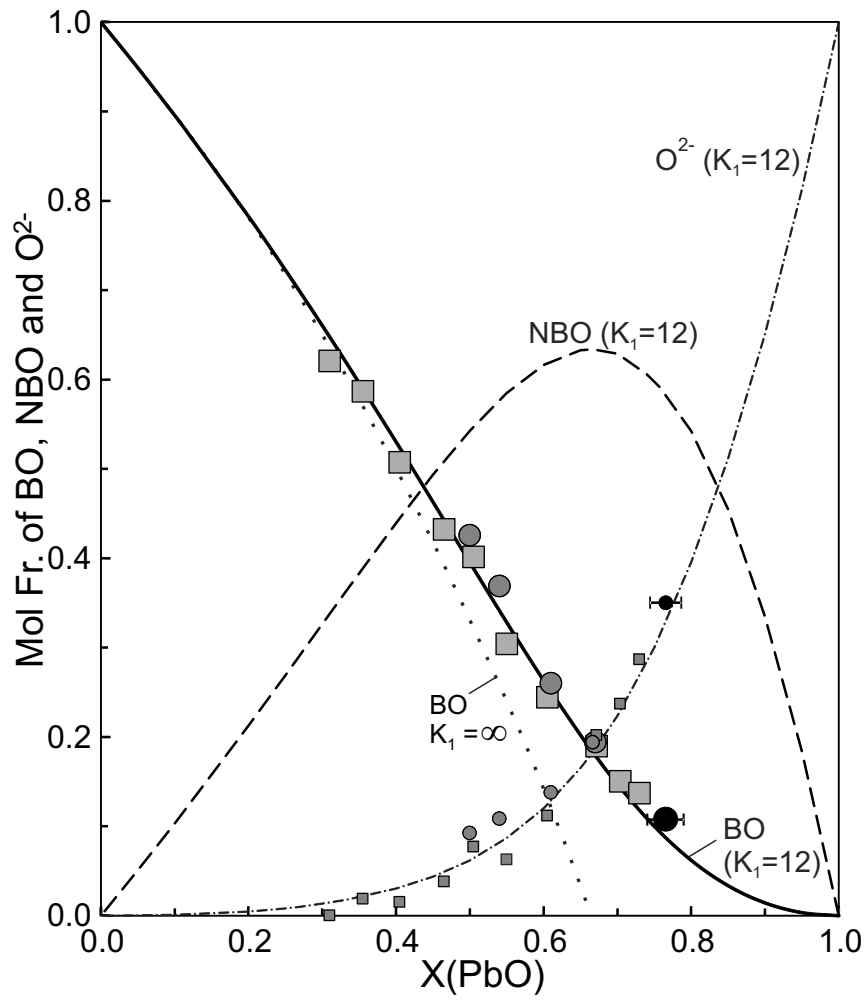
809   Fig. 3).
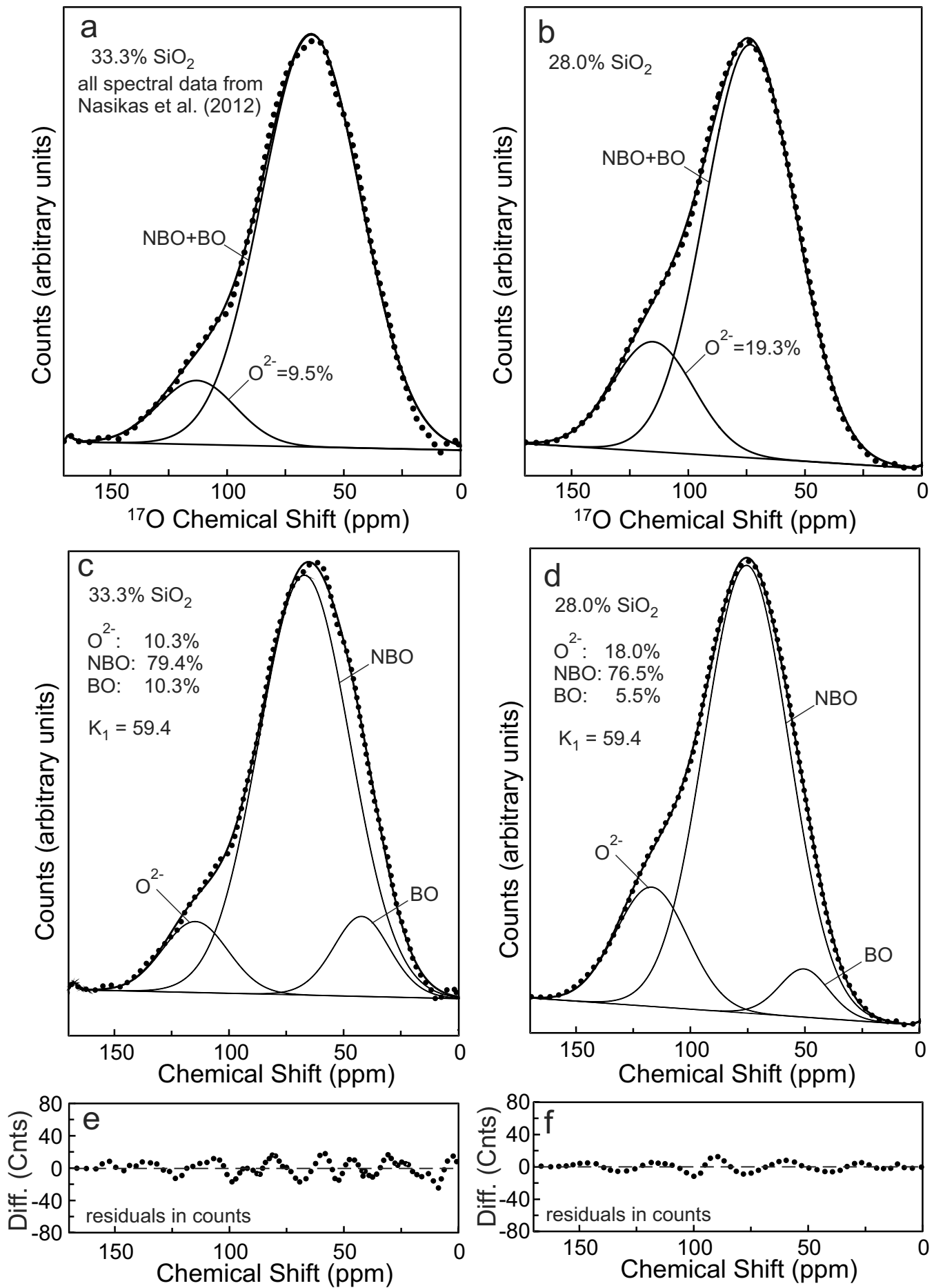
Fig. 1 - hwn

Fig. 2

Fig. 3 - hwn

Fig. 4 - hwn

Fig. 5 - hwn
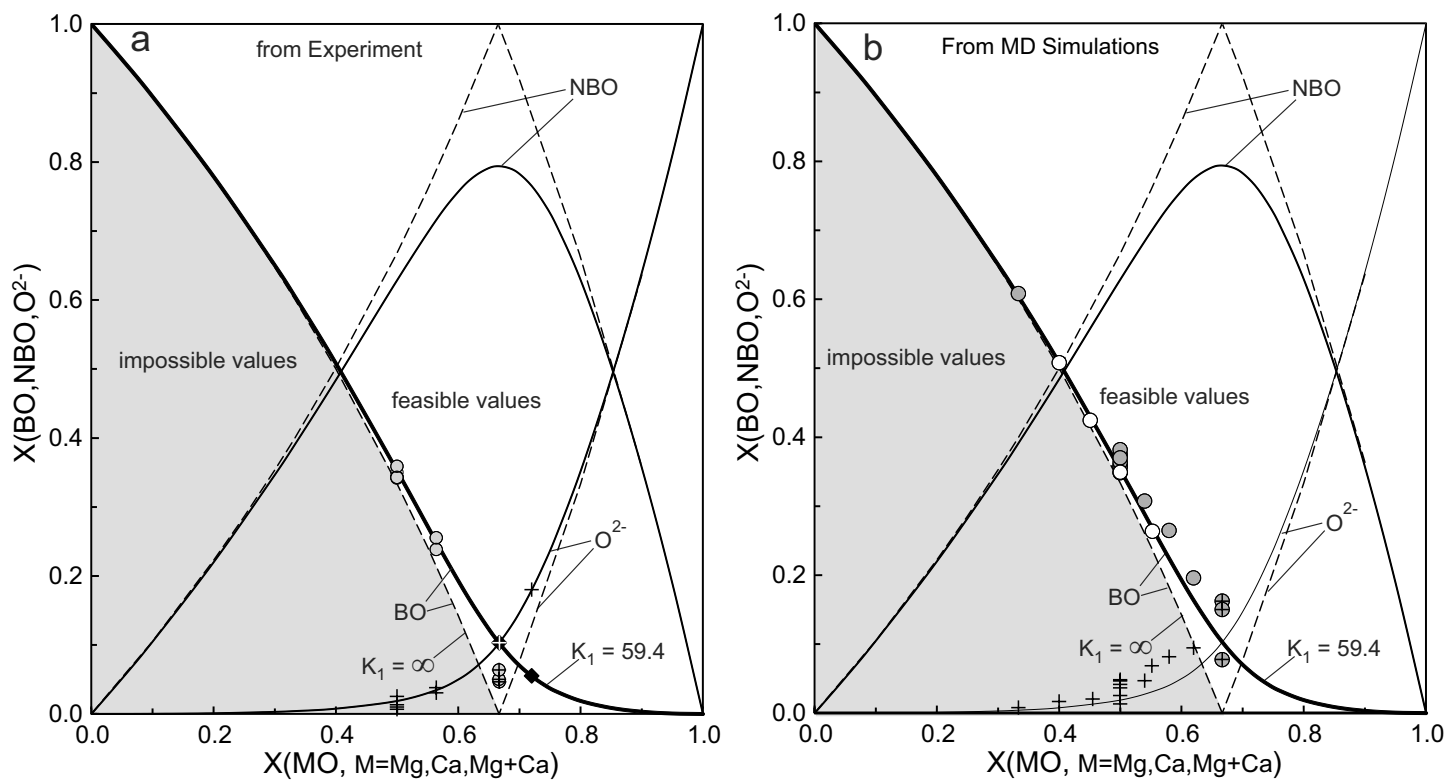
^{17}O NMR Spectrum of MgSiO$_3$ glass

(redrawn after Allwardt and Stebbins, 2004)

NBO

NBO = 57.4%
BO = 33.1%
?   = 9.5%

BO#1

BO#2

?

CPS (arbitrary units)

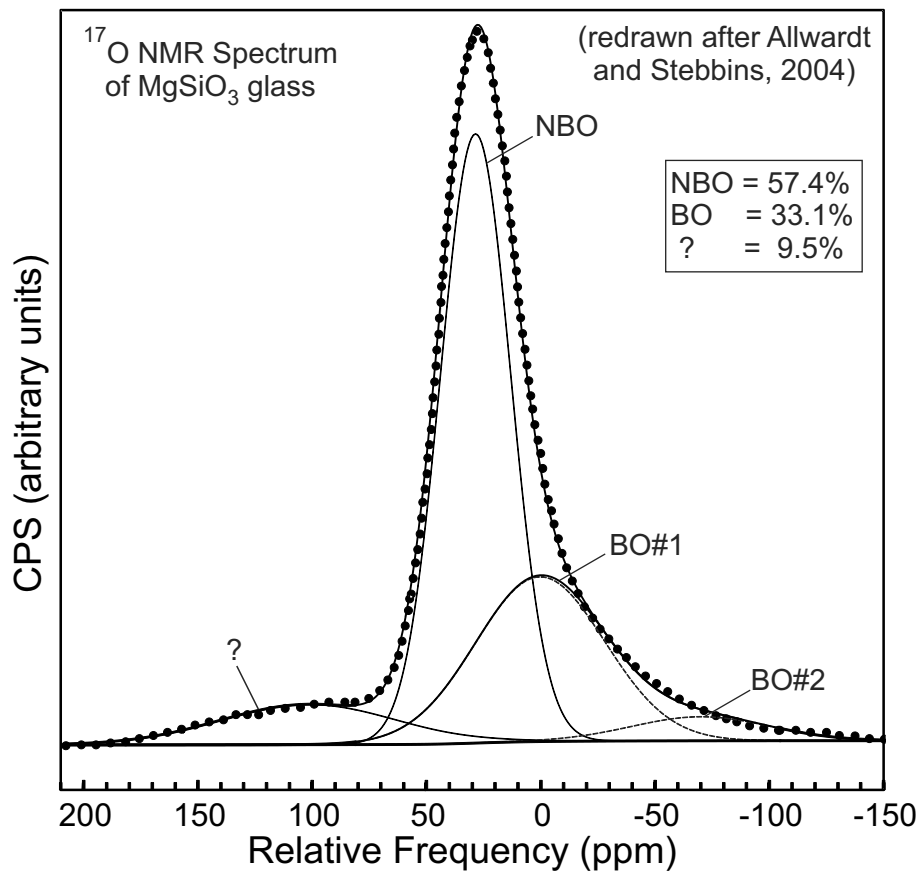200   150   100   50   0   -50   -100   -150

Relative Frequency (ppm)

Fig 6 - hwn
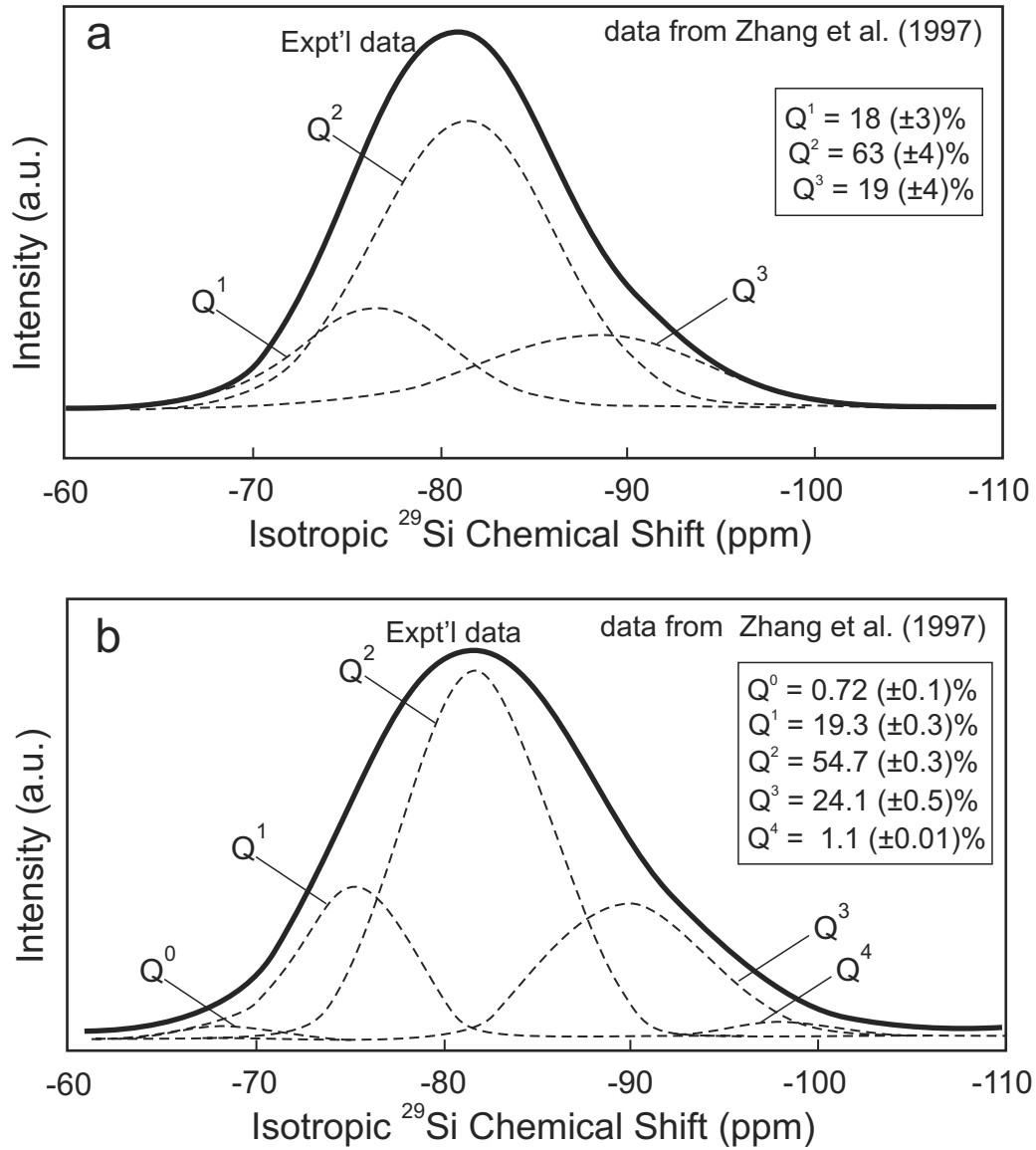
Fig. 7 - hwn

Table 1: BO, NBO and O^{2-} Peak Parameters from Fits to Spectra of Figs. 1, 2, 4 and 6

Figs. 1 and 2: O 1s XPS Spectral Results	Peak	Position (eV)	FWHM (eV)	Intensity (mol%)
Fig. 1c: BO FWHM constrained	BO	531.14	1.22	10.8
	NBO+O^{2-}	529.51	1.6	89.2
Fig. 2a: BO and NBO FWHM constrained	BO	531.01	1.22	14.7
	NBO	529.76	1.22	51.0
	O^{2-}	529.04	1.21	34.3
Fig. 2b: BO FWHM and peak areas constrained	BO	531.15	1.22	10.8
	NBO	529.71	1.52	54.2
	O^{2-}	529.22	1.41	35.0

Figs. 4 and 6: ^{17}O NMR Spectral Results	Peak	Position (ppm)	FWHM (ppm)	Intensity (mol%)
Fig. 4a: Unconstrained 2 peak fit to CM33 spectrum	BO+NBO	64.2	50.6	90.5
	O^{2-}	114.5	34.5	9.5
Fig. 4b: Unconstrained 2 peak fit to CM28 spectrum	BO+NBO	73.4	45.4	80.7
	O^{2-}	115.1	40.8	19.3
Fig. 4c: Three peak fit to the CM33 spectrum	BO	41.9	29.5	10.3
	NBO	67.1	46	79.4
	O^{2-}	113.8	33.6	10.3
Fig. 4d: Three peak fit to the CM28 spectrum	BO	51.9	26.6	5.5
	NBO	75.4	43.5	76.5
	O^{2-}	116.5	37.7	18.0
Fig. 6: Three peak fit to Mg-metasilicate glass[1,2]	BO#1	0.38	66.6	28.6
	BO#2	-70.0	71.1	4.5
	NBO	28.6	36.1	57.4
	"?"	101.7	91.0	9.5
	O^{2-}	- -	- -	1.5

1 - The asymmetric quadrupole peakshape of BO was fit using two Gaussian peaks

2 - The O^{2-} mol% was calculated from total BO and NBO abundances (see text).

Table 2: O-species abundances derived from experimental studies and plotted on Fig. 5a[1]

Literature Source	X_{MgO}	X_{CaO}	X_{SiO2}	X_{BO}	X_{NBO}	X_{O2-}
Nasikas et al. (2012) NMR - from our fit (Table 1)	0.334	0.334	0.333	0.103	0.794	0.103
	0.360	0.360	0.280	0.055	0.765	0.180
Nasikas et al. (2011) Raman CaMg-silicate glasses	0.334	0.334	0.333	0.084	0.832	0.084
Davis et. al. (2011) NMR - Mg-silicate glasses	0.667		0.333	0.046	0.907	0.046
	0.500		0.500	0.343	0.646	0.010
Sen et al. (2009) NMR - Mg-silicate glasses	0.667		0.333	0.050	0.900	0.050
	0.500		0.500	0.359	0.616	0.026
Sen and Tangeman (2008) NMR Mg-silicate glass	0.667		0.333	0.064	0.872	0.064
Allwardt and Stebbins (2004) NMR - $MgSiO_3$ glass	0.500		0.500	0.360	0.625	0.015[2]
Sneider et al. (2000) NMR - CaMg-silicate glass	0.250	0.250	0.500	0.342	0.650	0.008
Thompson et al. (2012) NMR - from Sidebands		0.564	0.436	0.230	0.738	0.032
Thompson et al. (2012) NMR from peak areas		0.564	0.436	0.223	0.746	0.017
Zhang et al. (1997) NMR - Ca-metasilicate glass		0.500	0.500	0.343	0.648	0.009
Retsinas et al. (2013) Raman - CaMg-silicate glasses	0.250	0.250	0.500	0.422	0.578	0.062
	0.270	0.270	0.460	0.320	0.680	0.052
	0.290	0.290	0.420	0.264	0.736	0.064
	0.310	0.310	0.380	0.200	0.800	0.082
	0.320	0.320	0.360	0.153	0.847	0.074
	0.335	0.335	0.330	0.110	0.890	0.106
	0.340	0.340	0.320	0.074	0.926	0.097
	0.350	0.350	0.300	0.013	0.987	0.102
	0.360	0.360	0.280	0.013	0.987	0.136

1 - All results where X_{O2-} has a negative value are excluded (i.e., impossible results).

2 - This value was calculated assuming O^{2-} was under then NBO peak (see text).

Table 3: O-species abundances derived from MD simulations and plotted on Fig. 5b[1]

Literature Source	X_{MgO}	X_{CaO}	X_{SiO2}	X_{BO}	X_{NBO}	X_{O2-}
Al-Hasni & Mountjoy (2014) Mg-silicate glasses	0.667		0.333	0.162	0.676	0.162
	0.620		0.380	0.196	0.710	0.094
	0.580		0.420	0.265	0.654	0.082
	0.540		0.460	0.307	0.646	0.047
	0.500		0.500	0.375	0.583	0.042
Mountjoy et al. (2011) Mg-metasilicate glass	0.500		0.500			0.045
Spiekermann et al. (2013) Mg-silicate glasses	0.667		0.333	0.077	0.845	0.078
	0.500		0.500	0.382	0.570	0.048
	0.333		0.667	0.608	0.384	0.008
Sen et al. (2009) Mg-silicate glasses[1]	0.667		0.333	0.050	0.900	0.050
	0.500		0.500	0.359	0.616	0.026
Mead and Mountjoy (2006) Ca-metasilicate glass		0.500	0.500	0.343	0.647	0.010
Cormier and Cuello (2013) Ca-Mg-silicate glasses		0.500	0.500	0.347	0.640	0.013
	0.120	0.380	0.500	0.357	0.617	0.027
	0.380	0.120	0.500	0.363	0.600	0.037
	0.500		0.500	0.370	0.580	0.047
de Koker et al. (2009) Mg_2SiO_4 glass	0.667		0.333	0.150	0.700	0.150

1 - All results where X_{O2-} has a negative value are excluded.